MANIPULATION AND CONTROL OF COLLECTIVE BEHAVIOR IN ACTIVE MATTER SYSTEMS

A DISSERTATION SUBMITTED TO

THE GRADUATE SCHOOL OF ENGINEERING AND SCIENCE

OF BILKENT UNIVERSITY

IN PARTIAL FULFILLMENT OF THE REQUIREMENTS FOR

THE DEGREE OF

DOCTOR OF PHILOSOPHY

IN

PHYSICS

By

Erçağ Pinçe

October 2016

MANIPULATION AND CONTROL OF COLLECTIVE BEHAVIOR
IN ACTIVE MATTER SYSTEMS
By Erçağ Pinçe
October 2016

We certify that we have read this dissertation and that in our opinion it is fully adequate, in scope and in quality, as a dissertation for the degree of Doctor of Philosophy.

Giovanni Volpe(Advisor)

Evren Doruk Engin

Balázs Hetényi

Fatih Ömer İlday

Alper Kiraz

Approved for the Graduate School of Engineering and Science:

Ezhan Karaşan
Director of the Graduate School

ABSTRACT

MANIPULATION AND CONTROL OF COLLECTIVE BEHAVIOR IN ACTIVE MATTER SYSTEMS

Erçağ Pinçe
Ph.D. in Physics
Advisor: Giovanni Volpe
October 2016

Active matter systems consist of active constituents that transform energy into directed motion in a non-equilibrium setting. The interaction of active agents with each other and with their environment results in collective motion and emergence of long-range ordering. Examples to such dynamic behaviors in living active matter systems are pattern formation in bacterial colonies, flocking of birds and clustering of pedestrian crowds. All these phenomena stem from far-from-equilibrium interactions. The governing dynamics of these phenomena are not yet fully understood and extensively studied. In this thesis, we studied the role that spatial disorder can play to alter collective dynamics in a colloidal living active matter system. We showed that the level of heterogeneity in the environment influences the long-range order in a colloidal ensemble coupled to a bacterial bath where the non-equilibrium forces imposed by the bacteria become pivotal to control switching between gathering and dispersal of colloids. Apart from studying environmental factors in a complex active matter system, we also focused on a new class of active particles, "bionic microswimmers", and their clustering behavior. We demonstrated that spherical bionic microswimmers which are fabricated by attaching motile *E. coli* bacteria on melamine particles can agglomerate in large colloidal structures. Finally, we observed the emergence of swimming clusters as a result of the collective motion of bionic microswimmers. Our results provide insights about statistical behavior and far-from-equilibrium interactions in an active matter system.

Keywords: Active matter, Speckle light field, *Escherichia coli*, Bionic microswimmers, Active Brownian motion.

ÖZET

AKTİF MADDE SİSTEMLERİNDE KOLLEKTİF HAREKETİN KONTROL VE MANİPÜLASYONU

Erçağ Pinçe
Fizik, Doktora
Tez Danışmanı: Giovanni Volpe
Ekim 2016

Aktif madde sistemleri, termal dengenin uzağındaki ortamlarda yer alan ve enerjiyi yönlendirilmiş harekete dönüştüren aktif yapı taşlarından oluşur. Aktif ajanların birbirleriyle ve de girdikleri ortamla etkileşimleri sonucu uzun-erimli düzenin oluşumu ve kollektif hareket ortaya çıkar. Aktif madde sistemleri içerisindeki bu tür dinamik davranışlara örnek olarak bakteri kolonilerindeki desen oluşumu, kuşların sürü oluşturması ve yayaların oluşturduğu kalabalığın kümelenmesi gösterilebilir. Bütün bu fiziksel olaylar, termal dengenin uzağında gerçekleşen etkileşimlerden kaynaklanmaktadır. Bu olayları yönlendiren dinamikler henüz tam anlaşılmamış ve yeterince üzerinde çalışılmamıştır. Bu tezde, mekansal düzensizliğin, kolloidlerin oluşturduğu yaşayan aktif madde sistemindeki kollektif dinamiği değiştirmesi üzerinde nasıl bir rol oynadığını inceledik. Ortamdaki heterojenliğin seviyesinin, bakteri banyosunun içerisinde yer alan kolloid topluluğunun uzun-erimli düzenini etkilediğini ispatladık. Bakteriler tarafından kolloidlerin üzerine uygulanan denge-dışı kuvvetlerin, kolloidlerin toplanması ve dağılması arasındaki geçişte önemli olduğunu gösterdik. Karmaşık aktif madde sistemlerindeki ortam faktörlerinin incelenmesi haricinde, yeni bir aktif parçacık sınıfı olan "biyonik mikroyüzerlerin" ve onların kümelenme hareketinin üzerine yoğunlaştık. Hareketli *E.coli* bakterilerini melamin parçacıklarına yapıştırarak elde ettiğimiz küresel biyonik mikroyüzerlerin büyük kolloid yapıları oluşturabildiklerini gösterdik. Son olarak, biyonik mikroyüzerlerin kollektif hareketi sonucu yüzen yığınların oluşumunu gözlemledik. Sonuçlarımız, aktif madde sistemi içersinde yer alan aktif parçacıkların istatistiksel davranışları ve aralarındaki denge-uzağındaki etkileşimleri hakkında fikir vermektedir.

Anahtar sözcükler: Aktif madde, Benekli ışık alanı, *Escherichia coli*, Biyonik mikroyüzerler, Aktif Brown hareketi.

Acknowledgement

"*There are many interesting phenomena associated with vision which involve a mixture of physical phenomena and physiological processes, and the full appreciation of natural phenomena, as we see them, must go beyond physics in the usual sense. We make no apologies for making these excursions into other fields, because the separation of fields, as we have emphasized, is merely a human convenience, and an unnatural thing. Nature is not interested in our separations, and many of the interesting phenomena bridge the gaps between fields.*" reads Richard Feynman in his famous lecture series [1]. My work on the active matter research was an experimental realization of Feynman's outlook. During my PhD. studies, I was fortunate enough to find a cross-disciplinary path where I could go "beyond physics" and learn microbiological techniques which helped me to gain new perspectives in the field of study. I am glad that now I am ready for the next step and confident to go further on this path. I would like to credit all the people who helped me to reach this stage and contributed to this theis:

First, I would like to thank Giorgio and Giovanni Volpe for allowing me to work in their interesting scientific projects. I would also like to thank KPV Sabareesh and all the members of Soft Matter Lab. who helped me during my PhD. work.

I would like to thank the members of thesis monitoring committee, Bálazs Hétenyi and Alper Kiraz for their helpful comments and critical reviews during the regular TİK meetings. I would like to specially thank Alper Kiraz for coming all the way up from İstanbul to monitor and evaluate my scientific progress.

I am grateful to Evren Doruk Engin and Fatih Ömer İlday for being the members of the thesis committee. It was almost like a miracle to me to come across such a kind and talented scientist as Doruk, I was extremely lucky to have known him. I enjoyed every minute of the discussions we made about our joint project, *E. coli* and all other geeky topics. Thank you for all the support you showed me!

I am indebted to Fatih Ömer İlday for his mentorship and kind support when

I was about to drop the program and leave the scientific realm altogether. His vision and his tireless scientific endeavor motivated me to work harder and be a better scientist. It has been a pleasure for me to have known you. So long, and thanks for all the fish!

I would like to thank Serim Kayacan İlday and Onur Tokel for their keen friendship. I will miss our small talks. Thank you for the companionship!

I would like to thank Prof. John Sandy Parkinson from University of Utah for his helpful critics and suggestions about the culturing of *E. coli* strain RP437.

A large part of my PhD. studies involved practicing microbiological techniques and I spent a great deal of time in the bacteria laboratory in the Molecular Biology and Genetics department at Bilkent University. I would like to thank my friends there, Mutlu Erdoğan, Pelin Telkoparan Akıllılar and Bilge Kılıç, whose support have been invaluable to me. Also, I would like to thank Bircan Çoban, Şahika Cıngır Köker and Seniye Targen for their warm friendship.

I am grateful for a handful of people who shared my ambitions towards becoming a good scientist when I first started this journey in 2008 and who supported me all the way. I would like to thank Mahmut Horasan and Can Siyako who were there when I needed them.

All in all, the PhD. period in Bilkent has been the longest and toughest fight of my life. I was so lucky that I did not have to fight alone and I had the best corner team one can have. I am grateful to my brother and my "cornerman", Çerağ Pinçe for his support, patience, and enduring this fight alongside me. I am thankful to my mother, Belgin Çelebi, for staying strong and for all the things she had to go through to see me happy. I could not possibly finish this work without you.

"*Hak bildiğin yolda yalnız yürüyeceksin.*"
Tevfik Fikret.

"*Hiç kimseye ihtiyacımız yok. Tek ihtiyacımız çalışmak!*"
Mustafa Kemal Atatürk.

Contents

List of Figures

List of Tables

Chapter 1

Introduction

Physical systems containing active parts that show distinctive features as taking up energy from the environment and transforming it into mechanical motion can be defined as *active matter* [2–4]. The dissipation of the stored energy via the interaction of the parts with each other and with the environment can drive such complex systems to a far-from-equilibrium state. Emergent collective phenomena in complex systems require self-organization of active parts, and therefore sustainable energy input, for a coherent collective motion to occur. In the case of thermal equilibrium, the formation of ordered structures, such as crystals or liquids, can be understood in terms of equilibration dynamics. However, life is an intrinsically far-from-equilibrium process that features complexity and diversification. As Schrödinger noted in his famous book "*What is life?*" [5], living matter is under constant inward and outward flux of material so it cannot be isolated from its environment and its existence depends on the exchange of energy as an open system. Historically, Boltzmann was the first who analytically related order to entropy as a microscopic feature of matter [6]. His findings indicated that non-equilibrium processes might also generate order as in the case of equilibrium and physical structures that exist in far-from-equilibrium can be spontaneously formed. This idea constructs the essence of how living matter must stay in far-from-equilibrium conditions. Prigogine introduced the idea of "dissipative structures" where functional active parts of a complex system can

self-assemble into a larger construct in space and time [7]; thus, active matter can be understood as a dissipative structure and stands as a good model system to study non-equilibrium statistics of microscopic matter.

In this introduction, we will first summarize how self-organization in a far-from-equilibrium setting emerges and then provide some background information on self-propelling particles and microswimmers. Furthermore, we will define active Brownian motion and finally briefly discuss how collective motion emerges in active matter system.

1.1 Self-organization far from equilibrium

Self-organization is the formation of highly ordered structures arising from the interaction between a multiple of significantly simpler components. This phenomenon is observed in open systems that are driven far from equilibrium and is often driven by non-equilibrium fluctuations and feedback loops [7, 8]. There are various examples of self-organization in physics, chemistry and biology where the simple constituent elements of a complex system transform into an ordered structure by collective movement. Examples of self-organization phenomena in physics are spontaneous crystallization of liquids (see Fig 1.1(a)) [10], diffusion-limited aggregation of branching patterns during the electric break-down of solids (Fig 1.1(b)) [11, 12], Belousov-Zhabotinsky reaction-diffusion systems (Fig. 1.1(c)) [13, 14], percolation in disordered landscapes [15, 16] and emergence of Rayleigh-Bénard convection patterns (Fig 1.1(d)) [17] . In chemistry, colloidal crystals (Fig 1.1(e)) [18–20], self-assembled supramolecular structures [21, 22] and formation of liquid crystals [23] are examples of self-organization at microscale. Turing's morphogenesis [24], growth pattern of bacterial colonies (see Fig 1.1(f) for the growth pattern of *Paenibacillus vortex*) [25–27], and flocking behavior [28, 29] are examples of micro- and macroscale self-organization behavior in the biological realm.

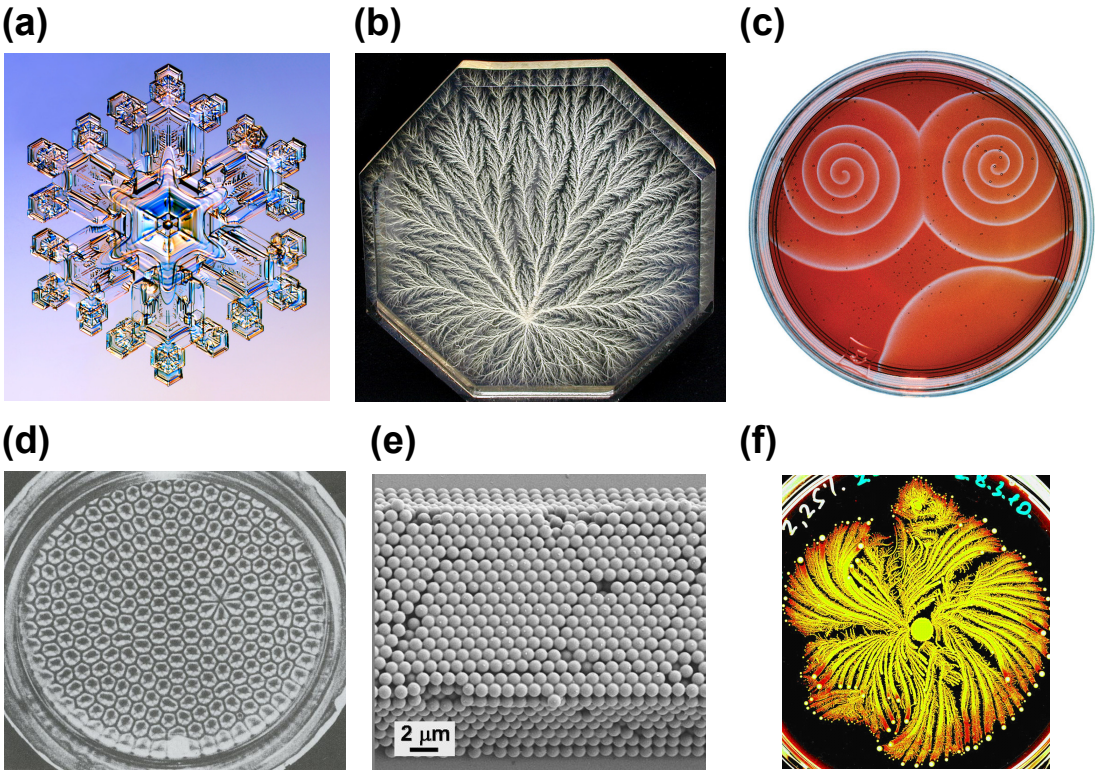

Figure 1.1: Self organization in nature. (a) Picture of an ice crystal. Crystallization of atoms occurs at near-equilibrium conditions. Reprint from http://www.snowcrystals.com. (b) The Lichtenberg figure, fractal patterns formed by the breakdown of dielectric inside plexiglass, is an example of diffusion-limited aggregation. Reprint from http://www.capturedlightning.com. (c) Belousov-Zhabotinsky reaction, an example of non-linear, oscillating chemical reaction which shows self-organizing patterns. Reprint from [9]. (d) Self-assembled Rayleigh-Bénard convection cells. Reprint from http://www.alderstone.com.(e) Picture of a colloid crystal. Reprint from http://www.nonmet.mat.ethz.ch. (f) The formation of *Paenibacillus vortex* colony on solid agar. Dentrite-like self-organized patterns can be clearly seen. Reprint from http://www.wikipedia.org.

1.2 Self-propelling particles

Self-propelling particles require a constant energy input to maintain the system in a far-from-equilibrium state. Such particles render the system to a far-from-equilibrium state by converting the energy resources, which are available in the environment, into a directed type of motion. As we mentioned in the previous section, active matter is formed by active constituents and these active constituents can spontaneously self-organize into an ordered matter. Self-propelling particles are the main constituents of such an organization. These small particles can be either inanimate, (e.g. nematics, artificial swimmers, robots) or living matter (e.g. microorganisms and humans). The first realization of an artificial flock in computer simulation was performed by Reynolds [30]. This artificial life simulation contains small agents (Boids for Bird-oid objects) modeling the flocking behavior of birds. Each boid follows a simple set of rules and is able to interact with other boids. The three basic rules of Boids model are separation of boids with each other at a critical proximity (Fig. 1.2(a)), alignment of the orientation of the local boids (Fig. 1.2(b)) and changing the position of a given boid towards the average position of its neighbors (Fig. 1.2(c)). As a result of this interaction, ensemble of boids featured large flocks and moved collectively. Reynolds' Boids model was the first simple model that emphasizes emergent complexity in swarming behavior of interacting agents. As in the case of Reynolds' model, Vicsek *et al.* constructred a novel type of swarming model where the particles are moving at a constant speed with random orientation [31, 32]. The *Vicsek model* is one of the earlier theoretical work to describe swarming in nature by using alignment interactions [29, 31]. The original version of Vicsek model is based on active particles moving with a constant velocity v adjusting their alignment with respect to the average alignment of neighboring members of the flock within an effective radius, typically on the order of flock's radius. An adapted version of Vicsek model can be described in terms of finite difference equation in two dimensions,

$$\begin{aligned} x_n(t+\Delta t) &= x_n(t) + v\Delta t\cos\varphi_n + \sqrt{2D_T\Delta t}\,\xi_{x,n} \\ y_n(t+\Delta t) &= y_n(t) + v\Delta t\sin\varphi_n + \sqrt{2D_T\Delta t}\,\xi_{y,n} \\ \varphi_n(t+\Delta t) &= \langle\varphi_m(t)\rangle \end{aligned} \tag{1.1}$$

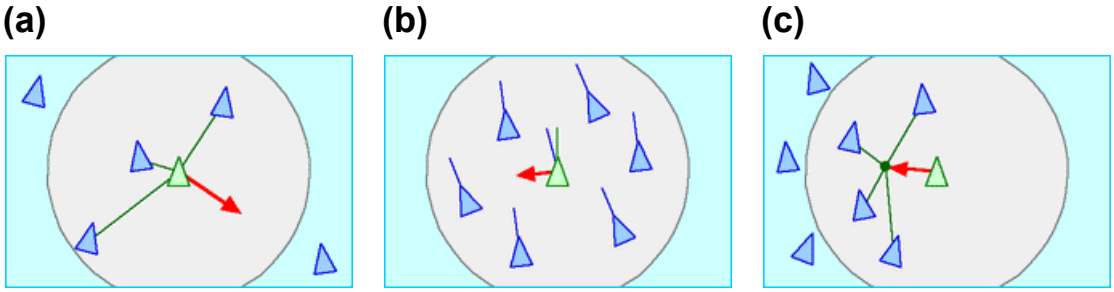

Figure 1.2: Three basic rules of Boids model. (a) Separation: avoiding the local boids crowding within flock radius (b) Alignment: directing towards the average orientation of the local boids. (c) Cohesion: change position towards the average position of the local boids. Reprint from http://www.red3d.com/cwr/boids/.

where φ_n is the orientation of particle n, $\langle\varphi_m(t)\rangle$ is ensemble averaged over all orientations of other particles within the flock at time t, D_{T} is the diffusivity of the particle and $\xi_{x,n}$, $\xi_{y,n}$ are white noise terms in x- and y-directions. The order parameters of the model are self-propelling particle density, $\rho = N/L^2$ where N is the number of particles and L is the size of the square shaped lattice that the motion of particles is translated by imposing periodic boundary conditions, v, the particles' speed and the intensity of the noise, η. For smaller particle densities and higher noise strength, particles starts grouping and move coherently as flocks in various directions. For higher particle densities and lower noise strength, the correlation between particles becomes long-ranged and the whole ensemble moves towards a specific orientation. This physical phenomenon is reminiscent of continuous phase transitions in thermal equilibrium. Active particles that are described by the Vicsek model start from a disordered state and swim into bands of coherent clusters. If active agents in the flock become suddenly passive ($< \vec{V} >= 0$) above a critical noise strength $\eta > \eta_c$, order between particles disappears [33,34]. Thus, active motion is crucial for flocking to occur. The most important feature of the Vicsek model is its universality: the emergence of collective phenomena does not depend on the species or a specific type of animal behavior that is controlled by using cognitive abilities. Therefore, this phenomenon might be observed on a group of inanimate active matter [35–38]. It is still a challenge for researchers to establish a unified theory for flocking self-propelling particles that correctly depicts collective phenomena in nature [29, 33].

Table 1.1: Examples of artificial microswimmers. Their propulsion mechanisms are summarized in the tables. Each letter corresponds to the microswimmer image given in Fig. 1.3.

	Microswimmer	**Mechanism of Propulsion**	**Fuel**	**Dimensions**	**Ref.**
(a)	Pt/Au self propelling rod-shaped particles	Oxygen formation due to decomposition of H_2O_2 at the Pt end of nanorod	3.3% H_2O_2	L = 1 µm ϕ = 370 nm	[39]
(b)	Pt capped spherical polystyrene (PS) Janus particle	Self-diffusiophoresis	1-10%H_2O_2	1.62 µm	[40, 41]
(c)	Gold capped Janus particles	Self-phoretic motion due to local demixing of the critical mixture by absorbed light	Critical mixture (e.g. water-2,6-lutidine)	0.1 to 10 µm	[42–44]
(d)	Polymeric spherical particles enclosing hematite cubes	Self-diffusiophoresis due to the decomposition of H_2O_2 near the particle surface by the incident UV light	3% H_2O_2	1.5 µm	[45–47]
(e)	Deformable cylindrical microrobots of liquid crystal elastomers	Particle locomotion due to deformation by photoizomerization and light-induced thermal effects	77mol% of mesogen + green laser light	L = 1 mm ϕ = 200 to 300 µm	[48]
(f)	3D printed PDMS based micro-scallops	Flapping magnetic shells by applying magnetic field	Externally applied magnetic field	$\sim$ 1.2 mm	[49]
(g)	Motile bacteria (e.g. *E. coli*) tethered spherical particles	Bacteria-powered swimming	Glucose (motility medium)	10 µm	[50, 51]
(h)	DNA-linked superparamagnetic colloids attached to red blood cells	Flagellar activity through the modulation of external magnetic field	Externally applied magnetic field	10 µm	[52]

A well-known example of self-propelling particles from living matter is the swimming microorganisms. Chemotactic microorganisms, such as *E. coli* can sense chemical gradients and respond to them by moving from regions with lower concentration of chemicals to regions with higher concentration or vice versa. Also, artificial self-propelling particles have been experimentally realized. Artificial microswimmers are colloidal particles which can harvest the energy stored in the environment in order to generate a directed self-propulsive motion.

Table 1.1 shows a list of artificial self-propelling particles and Figure 1.3 provides several examples of artificial particles which can be found in the literature. Unlike Brownian particles, the diffusion of active particles is not governed by forces in a thermal equilibrium setting. Thermal equilibrium dictates that fluctuations must be counterbalanced by the dissipative forces resulting from the drag of particles inside an aqueous medium. As a result of this effect, a Brownian particle experiences friction and its motion is eventually damped by the interaction with the environment because its kinetic energy is dissipated into heat by the surrounding molecules. This is a well-known consequence of the fluctuation-dissipation theorem imposing the reversible dynamics upon the system in terms of detailed balance [53, 54]. Therefore, the diffusion of Brownian particles must be invariant under time-reversal symmetry and obey detailed balance. On the other hand, individual trajectories of self-propelling particles break the time-reversal symmetry and show sensitivity to initial conditions because of irreversible dynamics of matter in a far-from-equilibrium setting. Besides their physical importance, artificial microswimmers have various applications regarding bioremediation, drug delivery [55–57], chemical detection [58] and environmental sustainability [59].

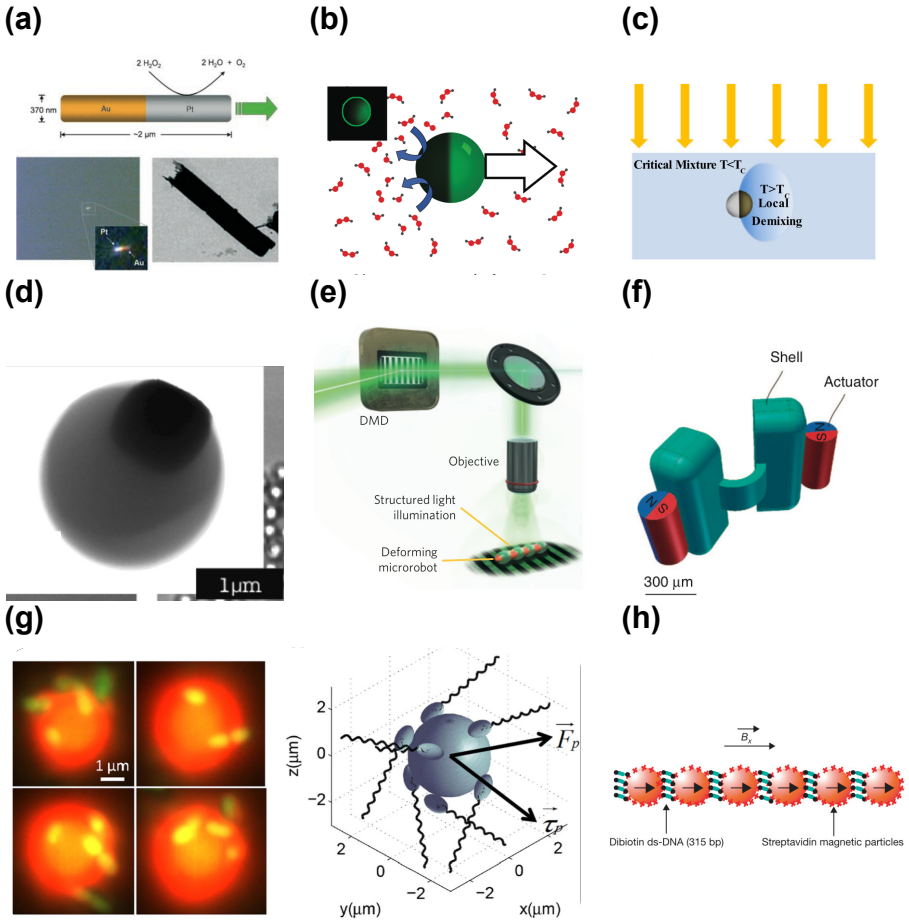

Figure 1.3: Examples to artificially realized microswimmers. (a) Pt and Au coated rod-shaped microswimmers which are actived when exposed to hydrogen peroxide solution due to decomposition of H_2O_2 at Pt interface. Reprint from [39]. (b) Pt capped spherical Janus particle that undergoes self-diffusiophoresis due to the concentration gradient around the particle surface. Reprint from [41].(c) Schematic of the self-propulsion mechanism of gold capped spherical Janus particle which performs a self-phoretic motion due to the local demixing of the critical mixture by the incident light. Reprint from [43]. (d) A Scanning electron microscopy image of polymeric spherical particles enclosing hematite cubes. Reprint from [45]. (e) Activation of deformable cylindrical soft-microrobot. Reprint from [48]. (f) A cartoon of 3D printed PDMS based micro-scallops. Reprint from [49]. (g) Florescent image of *E.coli* based microswimmers. Spherical PS bead is highlighted in red whereas attached bacterial cells are highlighted in yellow. Reprint from [51].(h) Schematic of DNA-linked superparamagnetic colloids as an artificial magnetic "flagellum". Reprint from [52].

1.3 Passive and active Brownian particles

In order to clearly understand how a single self-propelling particle diffuses in a homogenous environment, we have to first consider Brownian motion [60]. A single active particle having a velocity in a given direction is a good starting point to build the model of a self-propelling particle and compare it to the case of a Brownian particle. We can start to describe Brownian motion by considering the 1D Fokker-Planck equation for a given probability density function (PDF) $\rho(x,t)$,

$$\frac{\partial \rho(x,t)}{\partial t} = -\frac{\partial}{\partial x}[\mu(x,t)\rho(x,t)] + \frac{\partial^2}{\partial x^2}[D(x,t)\rho(x,t)] \tag{1.2}$$

where $D(x,t)$ is the spatiotemporal diffusivity of the particle and $\mu(x,t)$ is the drift term. We assume that there is no drift applied upon the diffusing particle ($\mu(x,t) = 0$) and the particle's diffusivity is uniform and constant over the infinitesimal time δt and space δx. Then, the Fokker-Planck equation (1.2) can be reduced into the 1D diffusion equation,

$$\frac{\partial \rho(x,t)}{\partial t} = D\frac{\partial^2 \rho(x,t)}{\partial x^2} \tag{1.3}$$

The exact solution of this equation for a Brownian particle located at the origin is a Gaussian function with zero mean and variance $2Dt$:

$$\rho(x,t) = \frac{1}{\sqrt{4\pi Dt}} e^{-\frac{x^2}{4Dt}} \tag{1.4}$$

If we consider a Brownian particle in one dimension starting its motion from the position $x = 0$, the PDF of its position at $t = 0$ is Dirac delta function peaked around the origin, $\delta(x)$, the first- and higher-order moments, except the second-order moment, of the position of vanish. The second moment of the position of the Brownian particle is calculated,

$$\langle \Delta x^2(t) \rangle = 2Dt \tag{1.5}$$

where $\Delta x = x(t) - x(t=0)$ and the brackets represent the ensemble average. For a Brownian particle moving in three dimensions, the second-order moment term becomes

$$\langle \Delta \mathbf{r}^2(t) \rangle = 6Dt. \tag{1.6}$$

As mentioned in the previous statement, both displacement and velocity average out to zero because of the symmetric Gaussian PDF. Hence, the second moment is a much more useful parameter to evaluate the average displacement of a diffusing particle. The expression in equation (1.5) is termed mean square displacement (MSD). It is also a measure of how far a particle can reach by performing Brownian motion in an given amount of time $\sqrt{t}$. To understand the meaning of MSD for diffusing particles, let us consider a dilute Brownian particle suspension in a viscous medium. According to Fick's first law, the diffusional flux of Brownian particles, $\mathbf{J}_{\text{diffusion}}$, at a position $\mathbf{r}$ is given by

$$\mathbf{J}_{\text{diffusion}}(\mathbf{r}) = -D\nabla\varphi(\mathbf{r}) \tag{1.7}$$

where D is the diffusivity, ∇ is the gradient operator and φ is the particle concentration in a unit volume [61]. We assume that there exists a uniform external potential field, $V(\mathbf{r})$, present in the medium. This potential field, $V(\mathbf{r})$, generates a conservative force field that acts on the Brownian particles in the liquid medium. We may assume that these particles respond to the force field by an opposite force term which is called the drag force, $\mathbf{F}_{\text{d}}(\mathbf{r})$, and given by

$$\mathbf{F}_{\text{d}}(\mathbf{r}) = \xi\, \mathbf{v}_{\text{d}}(\mathbf{r}) \tag{1.8}$$

where ξ is the friction coefficient and $\mathbf{v}_{\text{d}}$ is the drag velocity term. The Brownian

particle immersed in the viscous fluid experiences the drag force, $\mathbf{F}_{\mathrm{d}}$, and move with the drag velocity $\mathbf{v}_{\mathrm{d}}$. We can restate the drag velocity term as

$$\mathbf{v}_{\mathrm{d}} = \frac{-\nabla V(\mathbf{r})}{\xi} \tag{1.9}$$

where ∇ is the gradient operator. The particles will flow towards the minimum of the potential energy $V(\mathbf{r})$ with the drag velocity, $\mathbf{v}_{\mathrm{d}}$, and this creates a drift current, $\mathbf{J}_{\mathrm{drift}}$, due to the particle flux towards the minimum energy point

$$\mathbf{J}_{\mathrm{drift}} = \mathbf{v}_{\mathrm{d}}\, \varphi(\mathbf{r}) \tag{1.10}$$

and the total particle flux is given by

$$\mathbf{J}_{\mathrm{T}} = \mathbf{J}_{\mathrm{diffusion}} + \mathbf{J}_{\mathrm{drift}} \tag{1.11}$$

Under equilibrium conditions, the total flux must vanish and the particle concentration must follow the Maxwell-Boltzmann distribution, therefore the volume concentration can be approximated as $\varphi(\mathbf{r}) \propto e^{-\frac{V(\mathbf{r})}{k_B T}}$. Thus, equation (1.11) becomes

$$\frac{-\nabla V(\mathbf{r})}{\xi}\, \varphi(\mathbf{r}) = D \nabla \varphi(\mathbf{r}) \tag{1.12}$$

If we plug the expression for the particle concentration in equation (1.12), we obtain the Einstein-Smoluchowski relation [54, 62, 63],

$$D = \mu k_B T \tag{1.13}$$

where k_B is Boltzmann constant and T is temperature. Here μ is the mobility of the Brownian particle and inverse of the friction coefficient ξ. For a spherical particle with radius of R, the friction coefficient ξ is given by the relation,

$$\xi = 6\pi\eta R \tag{1.14}$$

according to Stokes' law. Here, η is the viscosity of the surrounding fluid. If we plug this coefficient into equation (1.13), we obtain the Stokes-Einstein-Sutherland equation for a Brownian particle in a low-Reynolds-number regime where viscous forces are dominant over inertial forces and the particle's inertia becomes negligible [62, 64],

$$D_{\mathrm{T}} = \frac{k_B T}{6\pi\eta R} \tag{1.15}$$

Equation (1.15) is the relation which connects mass diffusivity of a Brownian particle to physical and thermodynamical quantities. D_{T} is also termed as the translational diffusivity of a Brownian particle. The rotational diffusivity, D_{R}, can be retrieved by following the same line of reasoning only by changing the drag force friction coefficient ξ given in equation (1.14) to $\xi_{\mathrm{R}} = 8\pi\eta R^3$,

$$D_{\mathrm{R}} = \tau_{\mathrm{R}}^{-1} = \frac{k_B T}{8\pi\eta R^3} \tag{1.16}$$

where τ_{R} is the characteristic time scale for a Brownian particle subject to rotational diffusion. Einstein's model provided the framework needed to describe a Brownian particle's diffusion [62, 65]. However, the main drawback of this model was the lack of an accurate description of particle's instantaneous velocity and the role that Brownian particle's inertia plays in the diffusion. For example, the mean velocity of a Brownian particle can be defined

$$\langle v \rangle = \frac{\sqrt{\Delta x^2}}{t} = \frac{\sqrt{2D_{\mathrm{T}}}}{\sqrt{t}} \tag{1.17}$$

In equation (1.17), the mean velocity term $\langle v \rangle$ diverges when t approaches to zero, therefore $\langle v \rangle$ term cannot represent instantaneous velocity of a Brownian particle between two consecutive measurement taken place at an infinitesimal time intervals. The problem is based on the arbitrary selection of the time interval in which the instantaneous velocity of Brownian particle is calculated. According to Einstein, there is a short time interval during which the Brownian particle moves in a straight line, i.e., performs ballistic motion, and the instantaneous velocity can be measured within this short time scale $t < \tau_{\mathrm{m}}$. Einstein's model predicts that a Brownian particle of a 1 µm diameter in water would change its position in a time interval of 0.1 µs over a distance of about 2 Å before its speed and orientation are randomized by thermal noise [65, 66]. Recent technical advancements in optics made the measurement of a Brownian particle's position possible in a chamber filled with rarefied gas and in liquid medium for a spatial resolution down to 0.3 Å within a time frame of about 0.01 µs [67–69]. These findings verify the ballistic motion that the inertial Brownian particle experiences, confirming Einstein's intuition.

For an inertial Brownian particle, there must be a time interval $t < \tau_{\mathrm{m}}$ where the particle undergoes ballistic motion because of the inertial forces applied to the viscous medium by the massive particle. According to the equipartition theorem, in thermal equilibrium, each translational kinetic energy term of a massive particle corresponds to an average energy of $\frac{1}{2}k_BT$. Formulating the equipartition theorem for an inertial Brownian particle yields,

$$\langle v^2 \rangle = \frac{k_B T}{m} \tag{1.18}$$

In the ballistic regime ($t < \tau_{\mathrm{m}}$), the orientation and speed of the particle are not as largely fluctuating as in the case of non-inertial Brownian motion regime and therefore the speed of the particle can be taken as a constant. Thus, the MSD of a massive Brownian particle can be expressed as

$$\langle \Delta x^2(t) \rangle = \langle v^2 \rangle t^2 \tag{1.19}$$

if we plug the average velocity expression found in equation (1.18) into the MSD term above, equation (1.19) becomes

$$\langle \Delta x^2(t) \rangle = \frac{k_B T}{m} t^2 \tag{1.20}$$

which shows the MSD function of an inertial particle before momentum relaxation. Previously, in Einstein's model, the effect of inertia was neglected and the MSD function was linearly increasing as a function of time. Einstein's model neglected the effects of ballistics over a particle's trajectory and diffusion in smaller time intervals.

Langevin later showed that the linear trend for MSD of a Brownian particle is only valid for relatively large experimental times and ballistic effects cannot be ignored below a certain time threshold (i.e. the momentum relaxation time τ_{m}) from the onset of the motion. According to Langevin's model, the motion of a Brownian particle must be governed by Newton's second law and the total force acting upon the particle must include an external force as a drift term and a random force as a noise term. This simplified picture of Brownian motion provided Langevin a tool to probe single trajectories instead of dealing with the PDFs of particles.

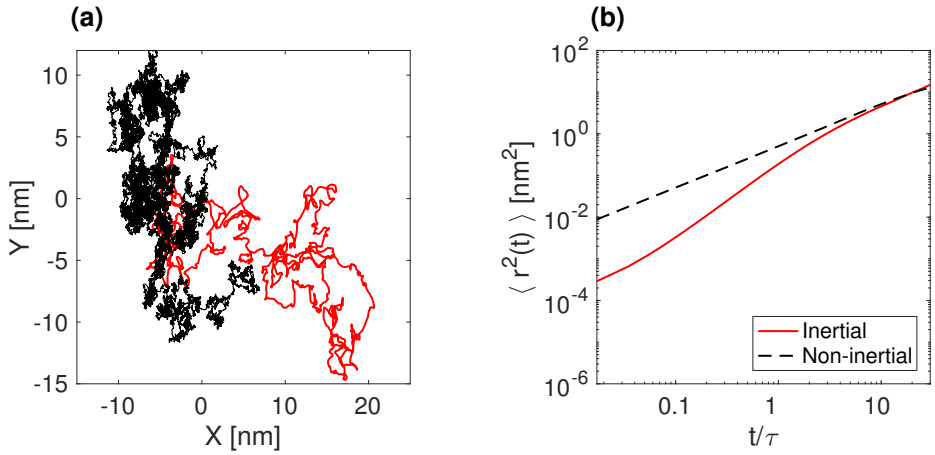

Figure 1.4: The effect of inertia on a Brownian particle. (a) Trajectory of a non-inertial Brownian particle (black) and a Brownian particle with inertia (red). The trajectory of the particle with inertia displays more directed motion compared to the massless Brownian particle. (b) The mean square displacement (MSD) plot of the Brownian particle with inertia in logarithmic scale. The MSD of the particle with inertia rapidly converges to the free diffusion line after the momentum relaxation occurs (i.e. $t \approx \tau$). The parameters of the particle with inertia that are used for this simulation are $R = 1\,\mu\text{m}$, $m = 11$ pg, $\eta = 0.001$ Pa s, T = 300 K and $\tau = 0.6$ s.

Langevin's equation for a massive particle is

$$m\frac{d^2x}{dt^2} = -\xi\frac{dx}{dt} + f(t) \tag{1.21}$$

where m is the mass of Brownian particle, $f(t)$ is the random force, i.e. the noise term and $\xi\frac{dx}{dt}$ is the friction term. The noise term can be defined as a white spectrum Gaussian noise corresponding to a delta-correlated random force in the time domain,

$$\langle f(t)f(t')\rangle = \delta(t-t'). \tag{1.22}$$

Again by using the equipartition theorem, the generic MSD function of an inertial Brownian particle can be deduced by ensemble averaging over many realization of the trajectories:

$$\langle \Delta x^2(t) \rangle = \frac{2k_B T}{\xi} \left(t - \frac{m}{\xi} + \frac{m}{\xi} e^{-\frac{\xi t}{m}} \right) \tag{1.23}$$

For time scales where the experimental time is larger than the momentum relaxation time ($t >> \tau_{\mathrm{m}} = \frac{m}{\xi}$), the MSD function recovers the free diffusion of a Brownian particle in Einstein's model,

$$\langle \Delta x^2(t) \rangle = \frac{2k_B T}{\xi} t = 2D_{\mathrm{T}} t \tag{1.24}$$

for smaller experimental times, i.e. $t << \tau_{\mathrm{m}}$ exponential term can be expanded into a power series for small t and the MSD of the particle becomes a quadratic function of time:

$$\langle \Delta x^2(t) \rangle = \frac{k_B T}{m} t^2 \tag{1.25}$$

Langevin's model successfully unified MSD of a massive Brownian particle for ballistic and diffusive regimes. Figure 1.4(b) shows the MSD function of inertial and non-inertial Brownian particles.

Microscopic particles are generally swimming in the low-Reynolds-number regime where viscous forces are dominant over inertial forces. Therefore, we shall neglect the inertial effects to model passive Brownian motion of a microscopic particle. The Langevin equations describing the motion of passive Brownian particle in two dimensions are

$$\begin{aligned} \dot{x} &= \sqrt{2D_{\mathrm{T}}}\, W_{\mathrm{x}}(t) \\ \dot{y} &= \sqrt{2D_{\mathrm{T}}}\, W_{\mathrm{y}}(t) \\ \dot{\varphi} &= \sqrt{2D_{\mathrm{R}}}\, W_{\varphi}(t) \end{aligned} \tag{1.26}$$

where x, y are the coordinates of the particle, φ is the angle showing the particle's

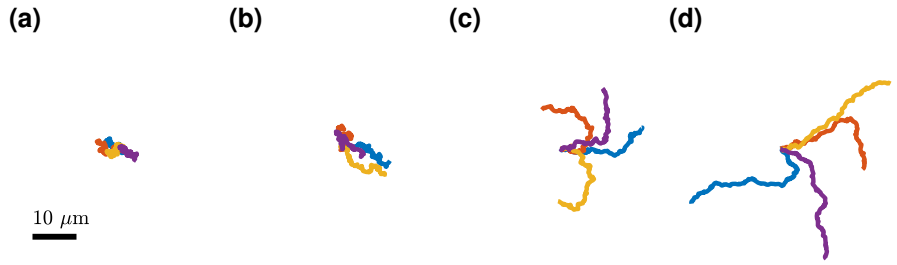

Figure 1.5: Simulating the motion of active Brownian particles in two dimensions. An active particle in a thermal bath having a velocity v and a orientation of ϕ with a radius of 1 µm undergoes Brownian motion. The motion of such a self-propelling particle is modeled as an interplay between Brownian and ballistic motion. Trajectories of active particles are shown with respect to their velocities.(a) $v = 0$ µm s^{-1}(Brownian particle), (b) $v = 1$ µm s^{-1}, (c) $v = 2$ µm s^{-1}, (d) $v = 3$ µm s^{-1}. Active particles with higher velocity explore larger area. Each trajectory corresponds to 11 seconds of simulation time. The direction of the active particle motion is randomized by the rotational diffusion at diffusive time scale larger than relaxation time $t >> \tau_{\mathrm{R}}$. Reproduced from [4].

orientation with respect to the center-of-mass frame, and $W_{\mathrm{x}}(t)$, $W_{\mathrm{y}}(t)$ and $W_{\varphi}(t)$ are independent, delta-correlated Gaussian noise terms. Simulated trajectories of non-inertial Brownian particles obtained by numerically solving Langevin equations with the finite difference method given as the set of equations (1.26) are shown in Fig. 1.4(a) [4, 70, 71]. In the case of an active particle, i.e. a self-propelling Brownian particle, the particle possesses a certain velocity v and is subject to rotational diffusion. The direction of the velocity vector determining the direction of motion is coupled to the particle's orientation (φ). Here is the set of equations governing the motion of an active Brownian particle [4, 71]

$$\begin{aligned} \dot{x} &= v\cos\varphi + \sqrt{2D_{\mathrm{T}}}\,W_{\mathrm{x}}(t) \\ \dot{y} &= v\sin\varphi + \sqrt{2D_{\mathrm{T}}}\,W_{\mathrm{y}}(t) \\ \dot{\varphi} &= \sqrt{2D_{\mathrm{R}}}\,W_{\varphi} \end{aligned} \tag{1.27}$$

Figure 1.5(a-d) shows a series of active particles starting their motion from the same point simultaneously. As the particle's velocity increases, the direction of motion changes because the particle is undergoing rotational diffusion. Thus, active particles follow a ballistic regime at smaller experimental time scales whereas

their motion becomes diffusive because of rotational diffusion at longer time scales. In order to underscore the contrast better between the notion of passive and active Brownian particles, let us go back to the concept of average trajectory and consider the motion of a particle starting from the axis origin with a specific orientation (i.e. $x(0) = 0$, $y(0) = 0$ and $\varphi(0) = 0$). For a passive Brownian particle, the average trajectory is identically zero, i.e. $\langle x(t)\rangle = \langle y(t)\rangle = 0$, simply because its PDF is symmetric (Gaussian function). However, introducing self-propulsion into the model breaks this symmetry in the radial direction. Since the Langevin equation for the particle's orientation φ is not coupled to the particle's coordinates, its angular PDF ($\rho_\varphi(x,t)$) must be the same expression as in the passive Brownian case, and therefore ensemble averages as $\langle\cos\varphi\rangle$ and $\langle\sin\varphi\rangle$ can be obtained by using the angular PDF. The ensemble average of sine term in $y(t)$ in equation (1.27) vanishes, thus the average trajectory in y-direction, $\langle y(t)\rangle$, identically vanishes [4]. The average velocity of a self-propelled particle in the x-direction can be calculated as

$$\langle x(t)\rangle = \frac{v}{D_\mathrm{R}}\left(1 - e^{-D_\mathrm{R}t}\right) \tag{1.28}$$

If we substitute radial relaxation time (τ_R), which is the inverse of the rotational diffusivity D_R, equation (1.28) becomes

$$\langle x(t)\rangle = \frac{v}{\tau_\mathrm{R}}\left(1 - e^{-t/\tau_\mathrm{R}}\right) \tag{1.29}$$

This expression shows that an active particle has a decaying memory of its initial orientation. An active Brownian particle starts its trajectory by following an initial direction for a finite *persistence length*, L, before its orientation is randomized by the rotational diffusion,

$$L = v\,\tau_{\mathrm{R}}. \tag{1.30}$$

The motion of a set of active particles with different velocities v, as shown in Fig. 1.5, displays ballistic motion at shorter time scales and diffusive motion at longer time scales. The crossover between regimes occurs at relatively shorter relaxation times for active particles with lower velocity v. In order to quantify this observation, we must derive the theoretical MSD function of an active Brownian particle as a function of its speed and characteristic time, τ_{R}. Theoretical MSD function for an active particle can be formulated as [40]

$$\langle \Delta x^2(t) \rangle = [4D_{\mathrm{T}} + v^2\tau_{\mathrm{R}}]\,t + \frac{v^2\tau_{\mathrm{R}}^2}{2}\,[e^{-t/\tau_{\mathrm{R}}} - 1] \tag{1.31}$$

At shorter time scales, $t << \tau_{\mathrm{R}}$, the MSD function of an active particles becomes linear as in the case of a non-inertial Brownian particle, i.e. $\langle \Delta x^2(t) \rangle = 4D_{\mathrm{T}}t$. Near to the crossover where the experimental time becomes comparable to the relaxation time, $t \approx \tau_{\mathrm{R}}$, the MSD function becomes quadratic, $\langle \Delta x^2(t) \rangle = 4D_{\mathrm{T}}t + 2v^2t^2$, and the motion regime of the particle is superdiffusive. At relatively longer times scales, $t >> \tau_{\mathrm{R}}$, the MSD function relaxes back to linear, $\langle \Delta x^2(t) \rangle = [4D_{\mathrm{T}} + 2v^2\tau_{\mathrm{R}}]\,t$, and the particle features enhanced diffusion with an effective diffusivity $D_{\mathrm{eff}} = D_{\mathrm{T}} + \frac{1}{2}v^2\tau_{\mathrm{R}}$. Figure 1.6 shows the MSD functions of passive and active Brownian particles with different velocities.

In this section, we studied the active Brownian particle model in 2D by introducing a self-propulsion velocity of the particle which is coupled to its orientation due to the rotational diffusion. In the following section, we shall discuss the Chiral active Brownian model describing the motion of asymmetrical active particles.

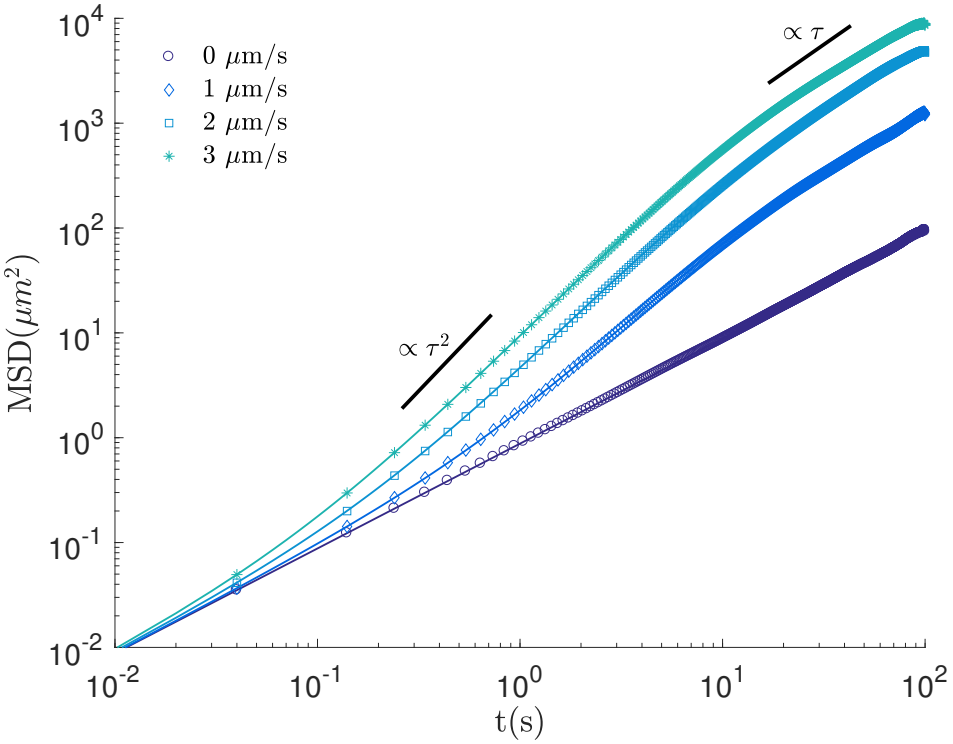

Figure 1.6: The enhanced diffusion and mean square displacement(MSD) of active Brownian particles. The lines show theoretical MSD functions whereas symbols show the MSD values of numerically simulated particles (see eq.(1.22)) with velocities $v = 0$ $\mu\mathrm{m\,s^{-1}}$(circles), $v = 1$ $\mu\mathrm{m\,s^{-1}}$(diamonds), $v = 2$ $\mu\mathrm{m\,s^{-1}}$(squares) and $v = 3$ $\mu\mathrm{m\,s^{-1}}$(stars). In the Brownian case ($v = 0$), the particle is in free diffusion regime (MSD(t) $\propto$ t) whereas in the active Brownian case, particle is in diffusive regime at shorter time scales (MSD(t) $\propto$ t where $t << \tau_{\mathrm{R}}$) renders to superdiffusive regime (i.e. MSD(t) $\propto$ t^2 for $t \approx \tau_{\mathrm{R}}$) and then relaxes back to free diffusion (MSD(t) $\propto$ t where $t >> \tau_{\mathrm{R}}$) with an enhanced diffusion coefficient. Reproduced from [4].

1.4 Chiral active Brownian motion

Moving along a straight line is seldom realized by a swimmer in most of the situations. The deviations from the linear trajectory of a microswimmer undergoing ballistic motion breaks the left-right symmetry. As a result of this, a swimmer's trajectory can show a certain degree of helicity, i.e. chirality. The chirality of a swimmer depends on the directional sign where it turns, which can be either clockwise (dextrogyre) or anti-clockwise (levogyre). A chiral swimmer shows circular motion in two dimension and helicoids in three dimensions. The chiral motion of microorganisms was first observed by Jennings in 1901 [72]. Since then the chiral motion of *E. coli* [73, 74], spermatozoa [75] and other species of bacterial cells have been observed in 2D as well as the helicoidal motion in 3D. For instance, *E.coli* bacteria exhibit chiral motion near to a solid boundary or liquid-air interface [76, 77]. Moreover, *E. coli* can be trapped outside of an obstacle or near to a solid wall surface [78, 79]. Chiral motion is not limited to animate matter, it can be also observed in L-shaped self-propelling particles [44] or asymmetrical particles [80].

The features of chiral motion in active particles can be also captured by a minimalistic model as we showed in the previous case of active Brownian particles. Here, an angular velocity term ω will be added to the time evolution of particle's orientation φ along with the rotational diffusion of an active particle with a velocity v:

$$\begin{aligned} \dot{x} &= v\cos\varphi + \sqrt{2D_{\mathrm{T}}}\,W_{\mathrm{x}}(t) \\ \dot{y} &= v\sin\varphi + \sqrt{2D_{\mathrm{T}}}\,W_{\mathrm{y}}(t) \\ \dot{\varphi} &= \omega + \sqrt{2D_{\mathrm{R}}}\,W_{\varphi}(t) \end{aligned} \tag{1.32}$$

where the helicity of particle's circular motion (e.g. levogyre or dextrogyre) is determined by the sign of ω. Figure 1.7 shows the simulated chiral motion of active particles governed by equations (1.32). As shown in equation (1.16), the rotational diffusivity scales with R^{-3} and as the size of a chiral active particle decreases, the random effects of diffusion becomes dominant over the ballistic ones. This can be clearly seen in Figs. 1.7(a-c).

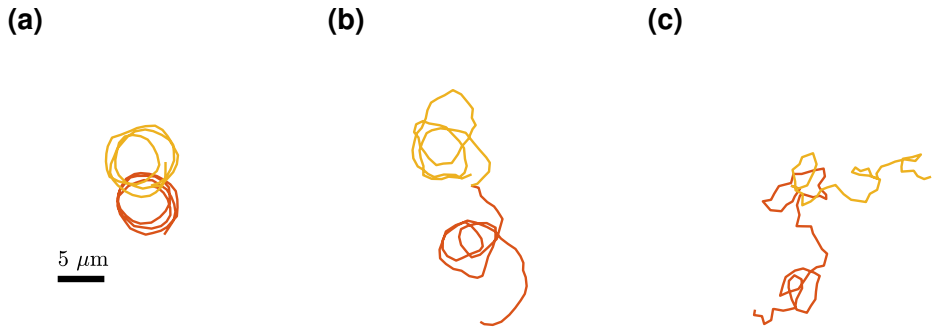

Figure 1.7: Simulating chiral active Brownian motion in two dimensions. An active Brownian having a constant angular velocity ω and linear velocity v will display chiral motion around a central external axis. (a-c) Simulated trajectories of chiral active Brownian particles with different helicities (i.e. dextrogyre (yellow/light gray) and levogyre (red/dark gray)). Each particle has linear velocity of $v = 30\ \mu\mathrm{m\,s^{-1}}$ and $\omega = 10\,\mathrm{rad\,s^{-1}}$ and radius of $R = 1000\,\mathrm{nm}$, $R = 500\,\mathrm{nm}$ and $R = 250\,\mathrm{nm}$ for (a), (b) and (c) respectively. For larger particle sizes, ballistic motion is dominant over diffusive effects. As the particle size is decreased, rotational diffusion becomes dominant over the directed motion because the rotational diffusion constant scales according to $1/R^3$ (eq. (1.12)). Reproduced from [4].

1.5 Collective behavior and clustering in active matter systems

So far, we have dealt with the dynamics of active Brownian particles in a homogeneous environment where there is no physical obstacle with which the particle can interact with. The particle's motion is governed by an overdamped Langevin equation as long as the particles are assumed to be swimming in a viscous fluid with a low Reynolds number. The presence of other active particles in the vicinity drastically change this physical picture because of the emergent interactions between swimming bodies. These interactions could be of hydrodynamical or steric (e.g. attractive or repulsive) nature. The onset of such interactions leads to dynamical changes on the single microswimmer level as well as on the collective level where phenomena such as dynamical clustering or phase separation in an ensemble of active particles might arise. We shall start by discussing how aligning interactions between active particles start the collective behavior and swarming in such an ensemble. As we mentioned in section 1.2, the Vicsek model is one of

the earlier theoretical works to describe swarming in nature by using alignment interactions [31]. Apart from the alignment-based flocking models, attractive and repulsive interaction between active particles might also lead to cluster formation. The phenomenology of this behavior follows from purely qualitative arguments: If two active particles collide with each other heads-on, each one is persistent to continue its course of motion. This two-particle aggregation can be broken only if one of the active particle's orientation points slightly away from the collision axis because of the rotational diffusion where the reorientation occurs within rotational relaxation time ($t \leq \tau_{\mathrm{R}}$). During this reorientation process, a third active particle might join a two-particle cluster if the mean-collision time is smaller than the time required for the reorientation of the active particles. Similar clustering dynamics was recently observed on light-activated hematite microswimmers. Palacci *et al.* experimentally showed dynamical clustering in the microswimmers enclosing an hematite core [45]. The formation of clusters is a dynamical process because of the constant particle scattering in and out of a given colloidal cluster. This interaction arises mainly due to the presence of attractive diffusiophoresis. However, a similar clustering behavior is observed in the settings where the role of diffusiophoresis on the attractive interaction between active particles is negligible [81–84]. The formation of active clusters is not limited to inanimate active matter, it is also observed in motile bacterial colonies [85, 86].

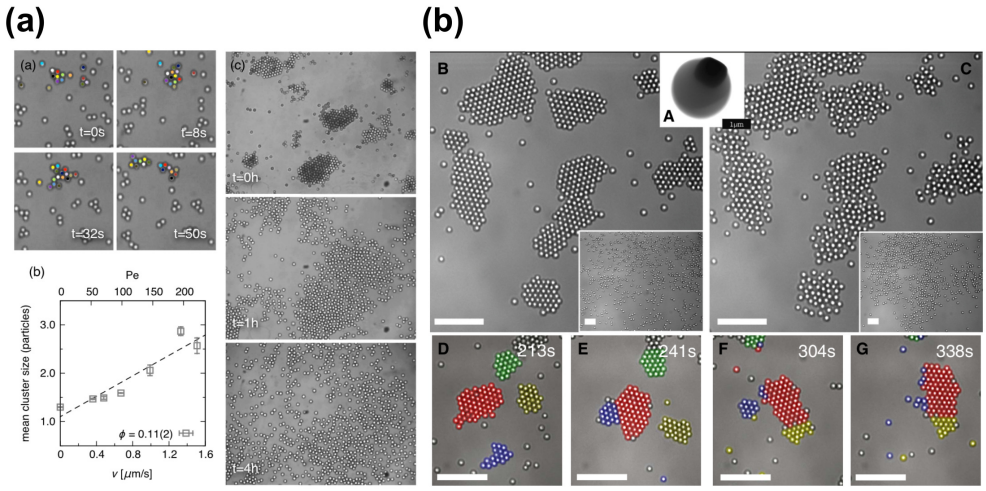

Figure 1.8: Examples to collective behavior and clustering in colloidal ensembles. (a) Clustering of light-activated active particles in aqueous medium. Colloids are interacting through short-range repulsive potentials leading to phase separation and other dynamic transitions (e.g. gas phase). Phoretic interactions between colloidal particles are negligible. Reprint from [81]. (b) Clustering of colloidal particles enclosing hematite cubes. In contrast to the previous example, attractive diffusiophoretic interactions play a role in the dynamical clustering of these active particles. Reprint from [45].

Chapter 2

Disorder-mediated crowd control in an active matter system

The spatial organization of individuals plays a crucial role in the growth and evolution of complex systems. Their gathering and dispersal are critical in phenomena as diverse as the genesis of planetary systems [87], the organization of ecosystems and human settlements [88], the growth of bacterial colonies and biofilms [89–92] the self-organization of active matter systems [45, 85] and the assembly of macromolecular complexes at the nanoscale [93, 94]. In systems close to thermal equilibrium, this phenomenon is observed in the formation and melting of crystals [95]. For systems that are far from equilibrium, such as living active matter, these dynamics become much less intuitive and can sensitively depend on environmental factors [3, 74]. Typical environments for natural active matter systems can indeed be highly heterogeneous, and, as recent theoretical work has shown [96, 97], the presence of spatial disorder can significantly influence the motility of active particles, thus leading an active system to different long-term behaviors. Despite these theoretical insights, the difficulty of experimentally exploring complex environments in a controllable way has held back the study of these dynamics in active matter systems. We have explored the long-term spatial organization of a population of colloids in an active bath under

diverse environmental conditions where a controllable degree of disorder is introduced with optical potentials [98, 99]. The colloidal particles are driven far from thermal equilibrium by an active bath of motile *E. coli* bacteria [100], which are self-propelling microorganisms whose motion proceeds as an alternation of running and tumbling events [101]; because of random collisions with the bacteria in the solution, the colloids are driven far from equilibrium, and, in a homogenous environment, their motion features a crossover at a characteristic time in the order of a few seconds from ballistic motion at short times to enhanced diffusion at long times with an effective diffusion coefficient that is higher for higher concentrations of bacteria [100]. The colloids in the active bath thus effectively behave like active particles [40, 102]. Differently from a system at equilibrium, our results show that the presence of spatial disorder in an external attractive potential alters the long-term dynamics of the colloidal active matter system: in particular, the depth of the local roughness in the environment regulates the transition between individuals gathering in and dispersing from the attractive potential, thus inspiring novel routes for controlling emerging behaviors far from equilibrium.

2.1 Results

2.1.1 Dynamics in smooth potentials

To set the stage, we first consider the simple configuration where we illuminate the colloidal particles (silica microspheres, diameter $d = 4.99 \pm 0.22$ μm) in a thermal bath, for example, in absence of bacteria, with a defocused Gaussian beam (wavelength $\lambda = 976$nm, waist $w_0 = 47.8 \pm 0.2$ μm, power $P = 100$ mW) whose intensity profile is reproduced in Fig. 2.1 (section 2.2 and Fig. 2.6). We tracked the motion of the colloids by digital video microscopy [103]; their trajectories over 1 minute preceding each snapshot are represented by solid lines in the time-lapse sequence in Fig. 2.1(b)-(d). The Gaussian beam generates a shallow smooth optical potential (Fig. 2.6) that attracts the colloids towards the

maximum of intensity in the centre of the illuminated area at an initial rate of 40.2 particles per minute (Fig. 2.1(e)); convection or thermophoresis are negligible for the wavelength, power and chamber geometry used in our experiments (section 2.2.5). In absence of non-equilibrium driving forces (i.e. in the absence of the bacterial bath), the particles form a crystal-like packed ordered structure within a few minutes from the activation of the potential (Fig. 2.1(d)) [95]. As the time-lapse sequence in Fig. 2.1(f)-(h) shows, the colloids gather at the bottom of the same attractive potential also in an active bacterial bath, albeit without forming a crystal-like structure (Fig. 2.1(h)). On average the particles drift towards the maximum of intensity, even though the stochastic nature of the active bath occasionally drives the colloids away from it, as demonstrated by their trajectories in Fig. 2.1(f)-(h); the overall result is that the colloidal population in the central region increases over time: within the first 30 minutes from the activation of the potential, the population increases from $N_{particles} \approx 20$ to $N_{particles} \approx 55$ as new individuals gather at a rate of 1.3 particles per minute (Fig. 2.1(i)). The effective radial drift, which is negative, also confirms the gathering of particles at the bottom of the potential (Table 2.1 and section 2.2.6). Since we start from a disperse solution of colloids and bacteria (section 2.2), we do not observe phase transitions [74] or the formation of active crystals [45, 85] within the time frame of our experiment.

2.1.2 Dynamics in rough potentials

To test the effect of spatial disorder on the active matter system, we now make the potential rough by generating an optical speckle pattern by mode-mixing a coherent laser beam in a multimode optical fibre (Fig. 2.1(j); section 2.2 and Fig. 2.6). Speckle patterns form rough, disordered optical potentials characterized by wells whose average width is given by diffraction (the average grain size, here $w_s = 4.87 \pm 0.70\ \mu m$) [98, 99]. Moreover, the well depths are exponentially distributed [98, 105], similar to the potentials found in many natural phenomena such as in the anomalous diffusion of molecules within living cells [106]. Since the

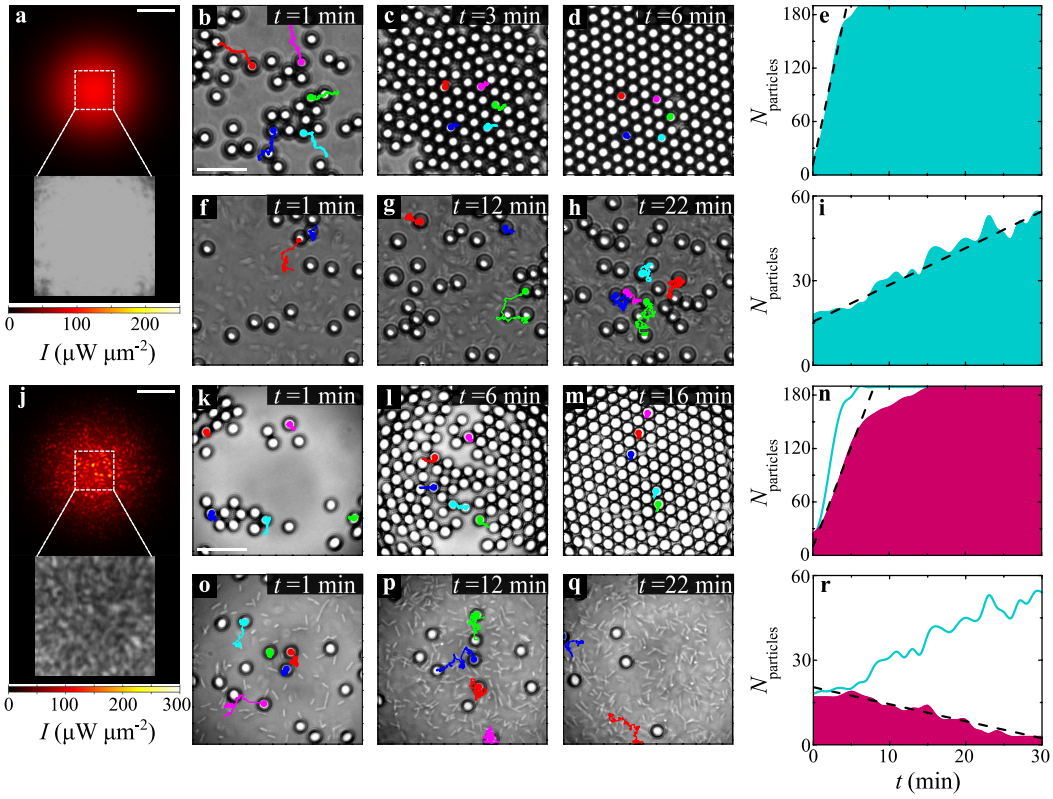

Figure 2.1: Gathering and dispersal of colloids in an active bath. In a smooth attractive optical potential generated by a Gaussian beam (λ = 976 nm, w_0 = 47.8 $\pm$ 0.2 mm and P = 100 mW) (a) the (b-d,f-h) time sequences show colloids (silica microspheres, $d = 4.99 \pm 0.22$ mm) gathering at the centre of the illuminated area (corresponding to the dashed square in (a,j)) in a thermal bath and in an active bath of *E. coli* bacteria, respectively. When disorder is added to this potential with a speckle pattern (j) the (k-m, o-q) time sequences show that colloids still gather at the centre in a thermal bath, but they are expelled from it in an active bath. The solid lines in the sequences show particles trajectories over 1 min before each snapshot; in each time sequence, trajectories with the same colour correspond to the same particle. The concentration of the bacteria as a function of time is similar in both sequences (f-h, o-q) in particular, it starts at a concentration $c_0 = 0.014 \pm 0.001$ cells per μm^2 and it reaches a plateau ~ 3.5 times this value as time passes. Sample experimental intensity distributions are shown in the insets in a and j. The shaded areas in e, i, n and r show the time evolution of the colloidal population for the four previous cases respectively. The dashed lines are linear fits whose slopes give the initial rate of particle gathering or dispersal. To directly compare smooth and rough potentials, the time evolutions of e and i are also shown as solid lines in n and r respectively. The scale bars correspond to 60 μm in a and j and to 20 μm in b and k. Reprint from [104].

fibre imposes a Gaussian envelope to the speckle pattern [99], this random optical potential has a global minimum, which, just as the smooth Gaussian profile, attracts the colloids towards the centre of the illuminated area (Fig. 2.6). In absence of bacteria, in fact, the colloids gather at the centre of the illuminated area and eventually form a crystal-like ordered structure as shown in the time-lapse sequence in Fig. 2.1(k)-(m). Compared with the sequence in Fig. 2.1(b)-(d), this process happens at a slower rate of 22.4 particles per minute (Fig. 2.1(n)), because the colloids are metastably trapped by the high-intensity grains of the static speckle pattern and undergo a process of transient subdiffusion (section 2.2) [98], as confirmed by the fact that the 1-min trajectories in Fig. 2.1(k) are much more confined than those in Fig. 2.1(b).

In the active bath, because of the attractive nature of the optical potential, one would still expect to observe the colloids gather at the centre of the illuminated area as in all previous cases. Yet, the time-lapse sequence presented in Fig. 2.1(o)-(q) shows the opposite behavior where the colloids are expelled from the central illuminated area-this is our central experimental result. The particle trajectories in Fig. 2.1(o)-(q) clearly show that on average the particles move outwards, even though, as previously noted, there are instances of particles moving in the opposite direction as a consequence of the stochastic nature of this process. The corresponding colloidal population, which at the beginning (at the time of activation of the potential) is similar in number to that of Fig. 2.1(f) ($N_{particles} \approx 2$), decreases to virtually no particle after 30 minutes at a rate of 0.6 particles per minute (Fig. 2.1(r)). The effective radial drift is positive and, thus, also confirms the dispersal of particles away from the illuminated area (Table 2.1 and section 2.2.6). These results clearly indicate that, while in absence of bacteria the colloids always gather at the bottom of any attractive potential and eventually form a crystal-like ordered structure [95], under the non-equilibrium driving forces introduced by the bacterial bath the colloids disperse if spatial disorder is added to the attractive potential. In the following, we explain these observations as a consequence of the presence of two sources of heterogeneity in the system: the first is the gradient in the local concentration of bacteria, and the second is the degree of local roughness of the attractive potential.

2.1.3 Underlying mechanism

To understand why the addition of spatial disorder leads the active system to this counterintuitive long-term response, we need to explore the underlying dynamics behind the behavior of the bacteria, which are the driving force that takes the system out of equilibrium and represent the first source of heterogeneity in the system. As it can be directly appreciated in the time-lapse sequences in Fig. 2.1(f)-(h) and in Fig. 2.1(o)-(q), the motile bacteria rapidly accumulate in the illuminated area following the activation of the optical potential. For the power levels we employ, the optical forces acting on the bacteria are negligible (section 2.2), whereas absorption of near-infrared light from the motility buffer generates a shallow temperature gradient ($\Delta T = 1.3 \pm 0.3$ K above room temperature; Fig. 2.8 and section 2.2.7) that attracts the bacteria towards warmer regions [92, 107–109]. To visualize the temperature profile, we calculated the steady-state temperature gradient for both smooth (Fig. 2.2(a), (b)) and rough potentials (Fig. 2.2(c), (d)).

The calculated temperature increase ($\Delta T \approx 1.2$ K above room temperature, section 2.2.7) agrees with the measured value and is similar for both potentials since it is mainly determined by the Gaussian envelope of the intensity profile and shows little sensitivity to the local roughness in the speckle case. As a consequence of their accumulation in the illuminated area, the bacteria form a concentration gradient that fades radially towards colder regions [92,107] so that the average velocity v of the colloids in the active bath also fades radially as a function of the concentration of bacteria (Fig. 2.2(e)) [100]. For both smooth and rough potentials, this creates an outward radial drift that tends to transport the colloids from regions of higher bacterial concentration (higher velocity) to regions of lower concentration (lower velocity), that is, away from the illuminated area. This is in agreement with the theoretical expectation that the density of active particles whose velocity is position-dependent scales with their velocity [110,111]. However, only when the colloidal dynamics are slowed down by the transient subdiffusion due to the disorder in the random optical potential (the second source of heterogeneity in the system) this outward drift of colloids outbalances their

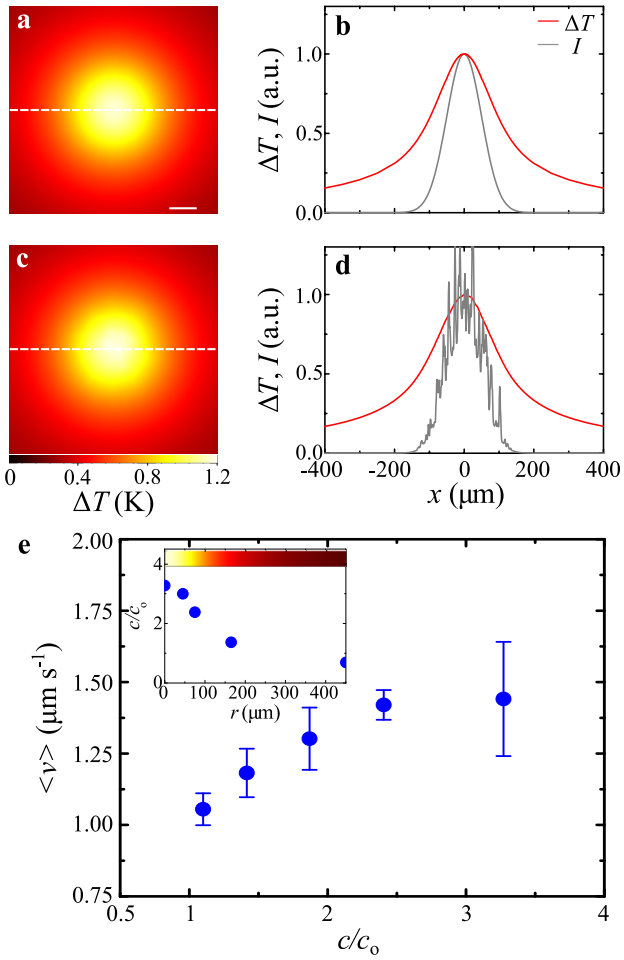

Figure 2.2: Colloidal average velocity in the temperature-induced gradient of bacteria. (a) Calculated temperature gradient ΔT near the surface due to light absorption in the motility buffer at $\lambda = 976$ nm for a Gaussian illumination. (b) Crosscuts of ΔT (red line) and of the Gaussian intensity profile I (grey line) along the dashed line in a. The scale bar corresponds to 40 µm. (c,d) Same as (a,b) for a disordered speckle illumination with a Gaussian envelope. In both cases, the temperature gradient is smooth and is mainly determined by the Gaussian envelope of the intensity distribution, despite the presence of local roughness in the speckle intensity. (e)*E. coli* bacteria are attracted towards warmer areas and their radial concentration c increases as a function of the local heating (inset), so that the average velocity v of the colloids, which depends on the concentration of bacteria, fades radially when moving away from the central illuminated area. c_0 is the concentration of bacteria before the activation of the optical potential and it is homogeneous in space. The error bars represent one s.d. around the average values. The colour bar in the inset shows the temperature variation as a function of position. Reprint from [104].

inward drift due to the attractive nature of the envelope of the optical potentials. In the bacterial bath, two competing effects influence the dynamics of the colloids: on the one hand, the attractive optical potentials induce a drift towards the centre of the illuminated area for both time-lapse sequences in Fig. 2.1(f)-(h) and in Fig. 2.1(o)-(q); on the other hand, the temperature-induced gradient of bacteria determines an opposite drift that tends to drive the colloids out of the illuminated area. On average, a single active particle would, in principle, settle where these two counteracting effects balance each other out; this will happen for both cases of smooth and rough potentials, even though at different positions. When multiple particles are present, however, crowding effects due to steric interactions come into play. In the smooth attractive potential (Fig. 2.1(f)-(h)), the particles drifting towards the centre of the illuminated area create a steric confinement that limits the capability of the particles already in the central region to escape from the potential well; hence the overall accumulation. In the rough attractive potential (Fig. 2.1(o)-(q)) instead, the local potential traps introduced by the disorder prevent the formation of a similar steric confinement by significantly slowing down the advancement of the outer, less-active particles towards the bottom of the potential well; hence the overall dispersal. Furthermore, once the particles are expelled, the same roughness created by the local traps is what prevents the particles to re-accumulate at the bottom of the potential well.These conclusions are corroborated by a set of experiments performed with a laser at $\lambda = 785$ nm where water absorption is about 20 times lower than at $\lambda = 976$ nm heating effects are thus negligible ($\Delta T \approx 0$ K). (Fig. 2.8 and section 2.2.7); in this case, we did not observe either accumulation of bacteria or dispersal of colloids, as shown in Fig. 2.3.

To test the generality of these results for a generic active matter system beyond the specific implementation of our experimental settings, we consider a minimalistic numerical model where the colloids are substituted by active particles whose average velocity v is position-dependent to account for the temperature-induced gradient of bacteria (section 2.2). This is a realistic scenario both for living and artificial active matter, for example, bacteria adjust their propulsion in response

to chemical gradients of food or toxins, and microswimmers in response to gradients in their energy source [74]. Figure 2.7 shows that, also in simulation, the long-term behavior of a population of active particles with a position-dependent velocity v depends on the underlying potential in quantitative agreement with our experimental results in Fig. 2.1: in a smooth Gaussian potential (Fig. 2.7(a)-(c)), the particles gather at its minimum at a rate of 0.88 particles per minute (Fig. 2.7(d)), while in a disordered potential with a Gaussian envelope (Fig. 2.7(e)-(g)) the particles are expelled from the central region at a rate of 0.26 particles per minute (Fig. 2.7(h)), despite the presence of attractive forces pushing them inwards.

2.1.4 Transition from gathering to dispersal

So far we have identified two long-term behaviours for the active system under different underlying potentials, that is, the gathering and dispersal of active particles. Figures 2.4 and 2.9 show that the transition between such opposite responses can be controlled by regulating the average depth of the local roughness in the potential. To decrease the potential depth in a controllable way, we generate time-varying speckle patterns with different decorrelation times τ_{s} (section 2.2 and Fig. 2.6): in this way, the effective potential is the time average of the potentials generated by all the M uncorrelated speckle patterns within the characteristic timescale of the colloids motion over the speckle patterns ($\tau_{\mathrm{p}} \approx 124$ ms) [98].

The change in local potential depth can then be measured by the speckle contrast $C_s = \frac{1}{\sqrt{2M}}$ where the factor 2 accounts for the two possible polarizations of light and $M = \frac{\tau_{\mathrm{p}}}{\tau_{\mathrm{s}}}$ for $\tau_{\mathrm{s}} \leq \tau_{\mathrm{p}}$ and $M = 1$ otherwise [105]. This allowed us to dynamically shift from a potential with maximum contrast when the speckle is static($C_s = 0.71$, $\tau_{\mathrm{s}} = \infty$, Fig. 2.4(a)) to a case where the speckle is decorrelating extremely fast so that any roughness is averaged out in time and the potential is essentially Gaussian ($C_s \approx 0$, $\tau_{\mathrm{s}} = 0.08$ ms, Fig. 2.4(i)). The evolution of the colloidal populations is shown in Fig. 2.4 for the various cases. As expected, the

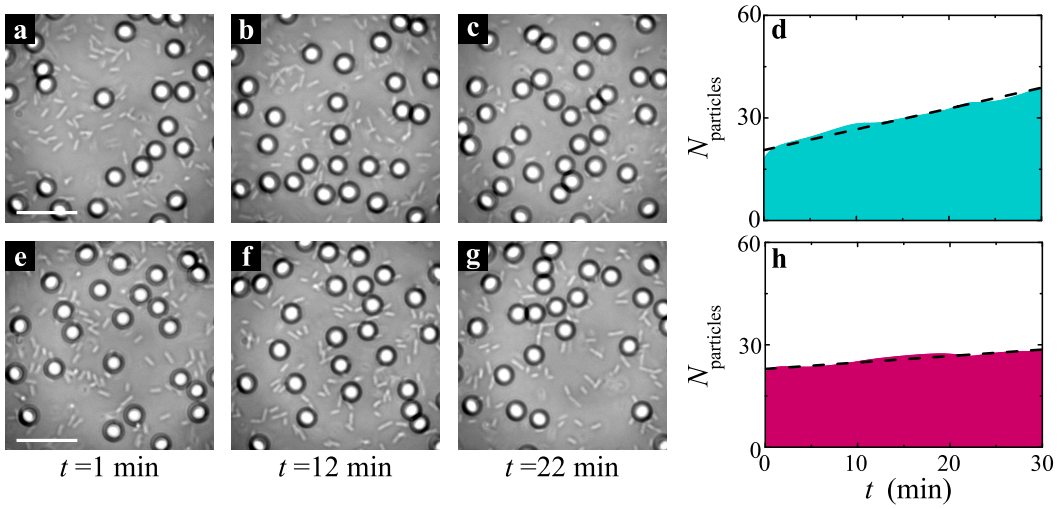

Figure 2.3: Colloidal dynamics in an active bath at 785 nm. The (a-c,e-g) time sequences show the gathering of colloids (silica microspheres, $d = 4.99 \pm 0.22$ µm) at the centre of the illuminated area in an active bath of E. coli bacteria for smooth and rough optical potentials generated by a laser at wavelength $\lambda = 785$ nm ($P = 100$ mW, $w_0 = 49.9 \pm 0.2$ µm). The average speckle grain size in e-g is $w_s = 4.38 \pm 0.50$ µm. Because water absorption is about 20 times lower at $\lambda = 785$ nm compared with water absorption at $\lambda = 976$ nm, heating effects are negligible and the gradient of bacteria that can drive the expulsion of colloids from the illuminated area does not form. This is in contrast to Fig. 2.1f-h, o-q at $\lambda = 976$ nm where bacteria are accumulating at the centre of the illuminated area and gathering of colloids in the active bath is observed only for a smooth potential (Fig. 2.1(f)-(h)), but not for a rough potential (Fig. 2.1o-q). The scale bars correspond to 20 µm. The shaded areas in d and h show the time evolution of the colloidal population for the two previous cases, respectively. The dashed lines are linear fits whose slopes give the rate of particle gathering, which is (d) 0.6 and (h) 0.2 particles per minute, respectively. Compared with the sequence in a-c the gathering of colloids in e-g is slowed down by the high-intensity grains of the static speckle pattern where the colloids are metastably trapped. Reprint from [104].

two extreme cases (Fig. 2.4(a), (i)) closely resemble the results of Fig. 2.1, and we respectively observe dispersal and gathering of colloids. For the intermediate cases, we observe a continuous transition between these two behaviours going through a case where the colloidal population is stable in time ($C_s = 0.05$, $\tau_s = 0.7$ ms, Fig. 2.4(h)) when the two competing processes, that is, the gathering and the dispersal of colloids are balancing each other. Interestingly, this transition is non-monotone: when we first reduce the contrast ($C_s = 0.13$, $\tau_s = 4.2$ ms, Fig 2.4(b) and $C_s = 0.1$, C_s, $\tau_s = 2.5$ ms, Fig. 2.4(c)) the dispersal of colloids becomes even faster before starting to slow down for lower values of C_s ($C_s = 0.07$, $\tau_s = 1.4$ ms, Fig. 2.4(g)). Our interpretation for this behavior is that initially, when the contrast of the speckle lowers and the average potential depth starts decreasing, the bacteria can push the colloids out of the local potential wells created by the speckle more easily, thus accelerating the rate of expulsion of the particles from the illuminated area. Finally, Fig. 2.5 shows that real-time control of the dynamics of the active system is achievable by changing the statistical properties of the potential. By switching between smooth and disordered Gaussian potentials and vice versa, the evolution of the colloidal population in time can be modulated and switched between opposite behaviors: in Fig. 2.5(a), the colloids gather in the central area in the first 15 minutes under smooth Gaussian illumination, and start dispersing as soon as the potential is switched to a disordered one; in Fig. 2.5(b) instead the colloids that are being expelled from the disordered attractive potential in the first 15 minutes restart accumulating as soon as the potential is switched to a smooth one.

2.1.5 Discussion

Our results demonstrate the critical role played by spatial disorder and environmental heterogeneity in determining the long-term behaviour of active matter systems as a result of non- equilibrium driving forces. The interplay between active particles and the features of the underlying potential where they move can lead to a transition between two long-term opposite behaviours, that is, the gathering and the dispersal of individuals from a common region.

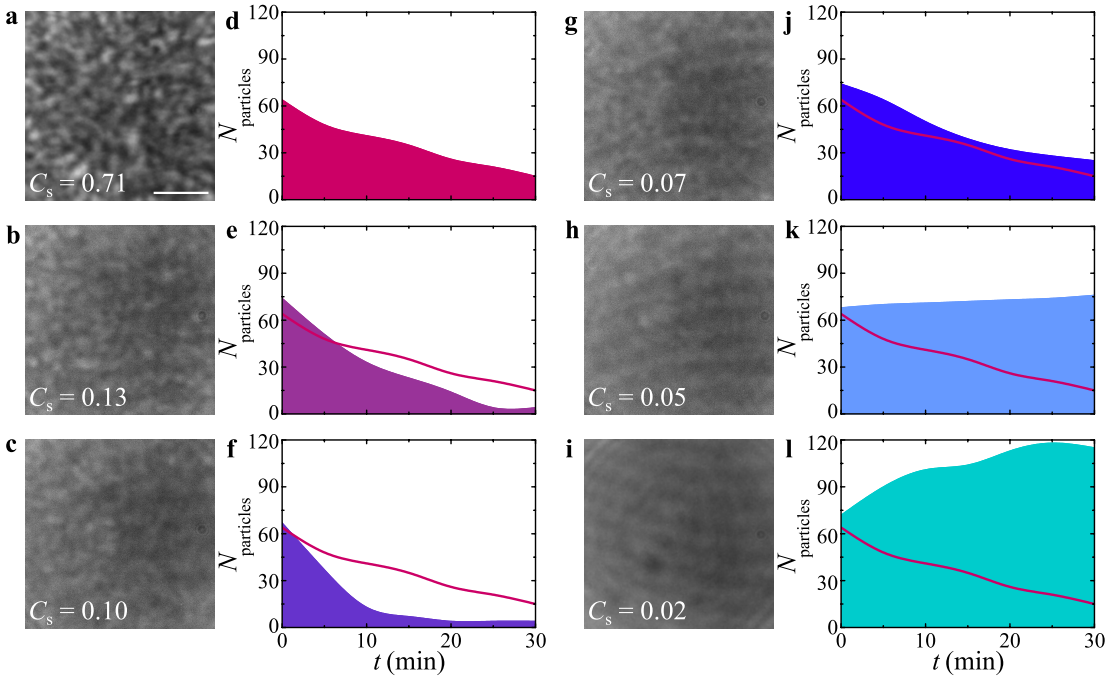

Figure 2.4: Controlled transition between gathering and dispersal of colloids in an active bath. (a-c,g-i) As the local roughness of the laser beam is continuously decreased from (a) a high-contrast speckle $C_s = 0.71$ to (i) an almost Gaussian distribution with very low-speckle contrast $C_s = 0.02$, the time evolution of the colloidal population in the active bath (d-f, j-l) show a non-monotone transition from (d) dispersal to (l) gathering of individuals in the central illuminated area. To directly compare all different cases, the time evolution in d is also shown as a solid line in the other time evolutions. The corresponding snapshots at $t =$ 30 minutes of the distribution of colloids are shown in Fig. 2.9. The scale bar corresponds to 20 µm. Reprint from [104].

Moreover, we have shown that these behaviors can be dynamically controlled by changing the statistical properties of the underlying potential in real time. In particular, we attribute our observations to the interplay among three ingredients, that is, multiple active particles with a position- dependent velocity (which in our experiment is generated by a gradient in bacterial concentration), an attractive potential, and a controllable degree of roughness in the potential, which allows a transition from the gathering of individuals in it to their dispersal. This effect can be explained as a combination of single- particle dynamics and steric collective interactions. While the single-particle dynamics are governed by an intrinsically out-of- equilibrium component associated to the drift in the gradient

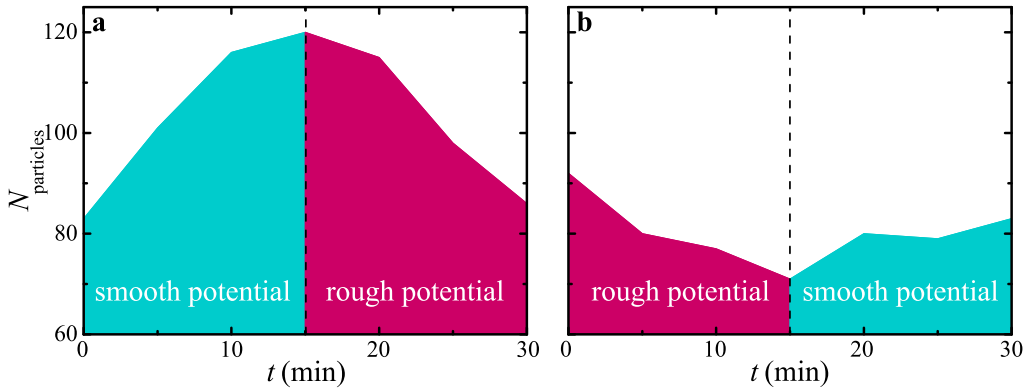

Figure 2.5: Dynamic switching between gathering and dispersal of colloids in an active bath. By dynamically controlling the roughness of the potential, it is possible to make the active system shift in real time between the two opposite behaviours in Fig. 2.4(d), (l). (a) The colloids first gather in the illuminated area under a smooth Gaussian potential, while they start to disperse after the first 15 min when the potential is switched to a disordered one. (b) The opposite situation is considered where the colloids, after dispersing for the first 15 minutes in a disordered potential, start gathering again in the illuminated area when the potential is switched to a smooth Gaussian one. Reprint from [104].

of the particle velocity, the collective interactions are not specific to active matter systems and they can also be observed for systems at equilibrium (for example, in the crystallization of colloids in a thermal bath in an attractive potential as in Fig. 2.1(b)-(d), (k)-(m)). Similar dynamics can determine the growth, health and survival of living matter systems such as bacterial colonies and biofilms where dispersal and aggregation of individuals play a central role in shaping the time evolution of the population [89, 91, 92]. In the study of active matter systems, other interesting phenomena can also emerge as a consequence of the individual or collective interaction of active particles with a disordered environment, such as their spontaneous trapping by disorder [96] or the emergence of other large-scale collective behaviors due to aligning interactions [112]. Beyond this fundamental interest, these results are relevant to engineer autonomous agents interacting with realistic (complex and crowded) surroundings, for example, artificial microswimmers capable of localizing, picking up and delivering nanoscopic cargos in catalysis, bioremediation, chemical sensing and drug delivery [113].

2.2 Methods

2.2.1 Bacteria preparation

Motile *E.coli* were cultured from the wild-type strain RP437 (*E. coli* Genetic Stock Center, Yale University). The bacteria were grown overnight at 32.5 °C in tryptone broth containing 1% tryptone. Once the culture saturated, it was diluted 1:100 into fresh growth medium and incubated again for 4 h at 32.5 °C while mildly shaken at 180 r.p.m. until the culture reached its mid-log phase (OD 600 $\approx$ 0.40). Finally, 5 mL of this dilution was centrifuged at 2,000 r.p.m. at room temperature for 10 min: the resulting precipitated bacterial pellets were then gently collected and resuspended in 5 mL of motility buffer containing 10 mM monobasic potassium phosphate (KH_2PO_4), 0.1mM EDTA(pH 7.0), 10 mM Dextrose($C_6H_{12}O_6$) and 0.002 % of Tween 20. This process was repeated three times for replacing the growth medium with motility buffer and halt bacterial growth completely.

2.2.2 Preparation of the solution of colloids

Diluted solutions of colloids in a thermal bath were prepared by adding 10 µL of monodisperse silica particles (Microparticles GmbH, diameter d = 4.99 $\pm$ 0.22 µm, volume fraction 0.025) to 990 µL of motility buffer. Diluted solutions of colloids in an active bath were instead prepared by adding 10 mL of monodisperse silica particles to 990 mL of motility buffer containing cultured *E. coli* bacteria.

2.2.3 Experimental set-up and optical potentials

All the experiments are performed on a homemade inverted microscope that is adapted to project both smooth and disordered optical potentials in the sample chamber [98, 114] as schematically shown in Fig. 2.6. Smooth Gaussian optical

potentials (beam waist $w_0 = 47.8 \pm 0.2$ µm are generated by focusing a Gaussian laser beam ($\lambda = 976$ nm, maximum output power $P = 600$ mW) with a planoconvex lens ($f = 50$ mm) onto the sample chamber (Fig. 2.6(a)). Wavelength and power ($P = 100$ mW) were chosen to generate a small increase in the temperature of the motility buffer without damaging the bacteria. Optical potentials with different degrees of disorder are generated by coupling the laser beam into a multimode optical fibre (core diameter 105 µm, numerical aperture (NA) = 0.22, 51-m long) using a planoconvex lens of short focal distance (f = 25.4 mm), as shown in Fig. 2.6(b). The typical output field, known as speckle, has a random appearance with a Gaussian envelope (beam waist $w_0 = 49.9 \pm 0.2$ µm) since it is the result of the interference of a large number of optical waves with random phases, corresponding to different eigenmodes of the fibre. In our experiments at $\lambda = 976$ nm, the average speckle grain size is $w_s = 4.87 \pm 0.70$ µm. The fibre is attached to a mechanical oscillator whose vibration frequency can be modulated to change the roughness of the optical potential [98]: when the oscillator is off, the speckle is static in time (decorrelation time $\tau_s = \infty$, Fig. 2.6(c)); otherwise, the frequency of the oscillation can be increased in a controlled manner to have a speckle that decorrelates faster and faster until any roughness is averaged out and the potential is a smooth Gaussian ($\tau_s = 0.08$ ms, Fig. 2.6(c)). By controlling the speckle decorrelation time between these two extremes, the average depth of the local roughness in the potential can also be controlled. It is worth noting that, for the smooth potential, we obtained qualitatively similar results, that is, gathering of colloids, with both versions of the set-up. The fibre output end is connected to a flat-terminated adapter (Thorlabs, SM1SMA) that constitutes the upper wall of the sample chamber containing the solutions of particles and bacteria; the distance between the top and the bottom of the chamber is $l \approx 100$ µm. In both versions of the set-up, the particles are tracked by digital video microscopy using the image projected by a microscope objective ($\times$ 20, NA = 0.5) on a monochrome charge-coupled device (CCD) camera with an acquisition rate in the range of $5-21.4$ f.p.s. [103]. Optical scattering forces push the particles in the direction of light propagation towards the lower wall of the sample chamber, so that they effectively confine the particles in a quasi-two- dimensional (2D) space. The incoherent illumination for the tracking is provided by a white-light lamp

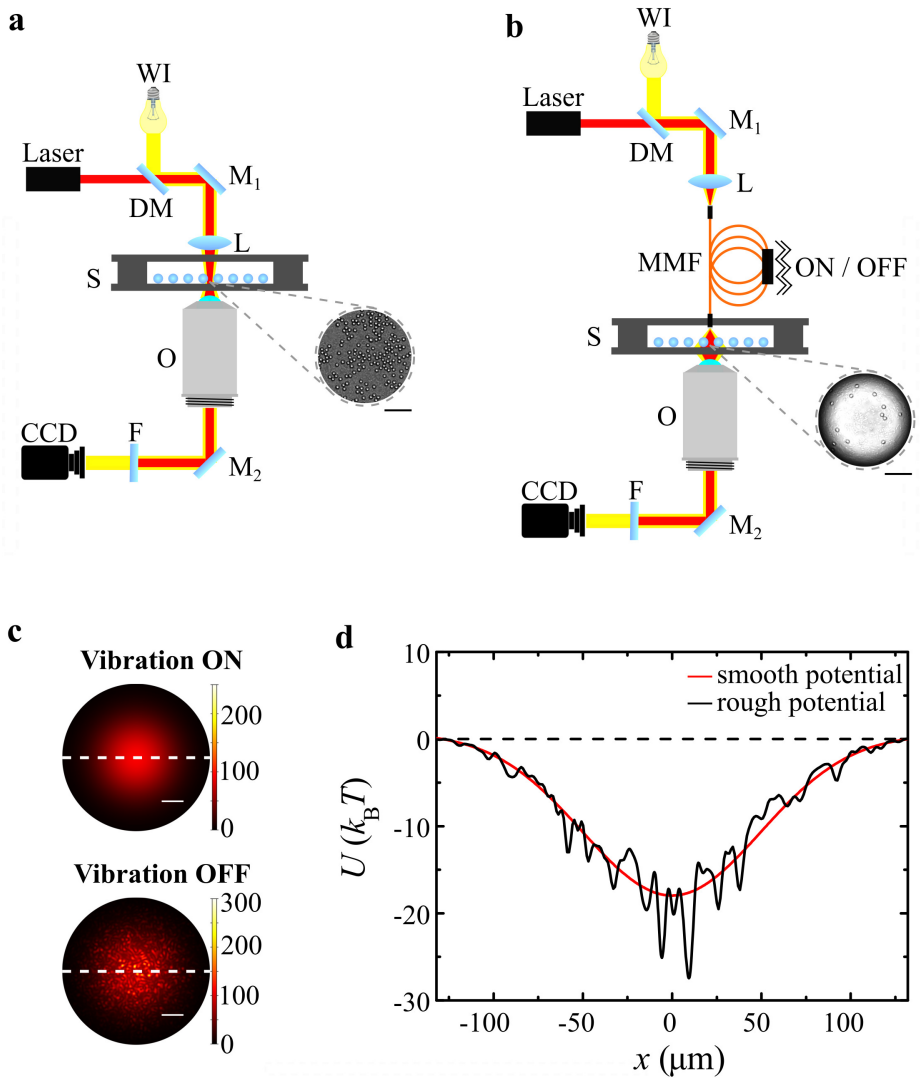

Figure 2.6: Schematics of the setup. Optical setups to generate (a) smooth Gaussian optical potentials and (b) optical potentials with a controllable degree of disorder: WI, white light lamp; DM, dichroic mirror; M_1 and M_2, mirrors; L, lens; S, sample; O, objective; F, filter; CCD, CCD camera; MMF, multimode optical fiber. (c) The fiber in b is attached to a mechanical oscillator whose vibration frequency can be modulated to change the roughness of the optical potential. (d) The profiles of the optical potentials along the white dashed lines in c both for smooth Gaussian illumination (red line) and disordered illumination (black line). All scale bars correspond to 40 μm. Reprint from [104].

either directly projected onto the sample (Fig. 2.6(a)) or coupled into the optical fibre (Fig. 2.6(b)) using a dichroic mirror (Thorlabs, DMLP605). The typical duration of an experiment is ~ 60 minutes before bacteria motility starts to decrease because of lack of oxygen and nutrients. Fig. 2.6(d) shows examples of calculated optical potentials for the colloidal particles corresponding to the level of power used in the experiments for both Gaussian and random illumination [99, 115]. Due to their Gaussian envelope, both potentials show a global minimum at their centre several times deeper than the characteristic thermal energy ($\sim$18 k_BT). The potential corresponding to random illumination also presents several local minima on its Gaussian envelope that are deep enough ($\approx 4\ k_BT$ on average for a static speckle) to metastably trap the colloids in the high-intensity grains of the speckle. For the bacteria (for the same levels of power), the global minimum of the Gaussian envelope in the optical potentials is in the order of $\approx 0.05\ k_BT$ and the local minima on the Gaussian envelope of the rough potential are in the order of $\approx 0.3\ k_BT$. Both global and local minima are significantly smaller than the thermal energy, thus optical forces on bacteria can be safely neglected.

2.2.4 Numerical model

We consider a numerical model where the colloids in the active bath are represented by self-propelled hard spheres of radius r that move responding to the following set of Langevin equations [71]:

$$\begin{aligned} \frac{d}{dt}\phi(t) &= \sqrt{\frac{2}{\tau_{\mathrm{r}}}}W_{\phi} \\ \frac{d}{dt}x(t) &= v\cos\phi(t) + \sqrt{D_{\mathrm{SE}}}\,W_{\mathrm{x}} + F_{\mathrm{x}}(x,y) \\ \frac{d}{dt}y(t) &= v\sin\phi(t) + \sqrt{D_{\mathrm{SE}}}\,W_{\mathrm{y}} + F_{\mathrm{y}}(x,y) \end{aligned} \tag{2.1}$$

where $[x(t),y(t)]$, $\phi(t)$, v, τ_{r}, D_{SE}, $\gamma = 4\pi vr$ are, respectively, the active particles position, orientation, velocity, rotational diffusion time, Stokes-Einstein diffusion coefficient and friction coefficient; v is the viscosity of the surrounding

medium; and W_ϕ, W_x and W_y are independent white noise processes [71]. Therefore, to model the effect of the bacteria on the motion of the colloids, in addition to Brownian motion, the spheres move with a radially-dependent velocity $v(r)$ in a direction that changes randomly on a timescale determined by an effective rotational diffusion τ_r [71]. The position-dependent velocity of the active particles accounts for the fact that, in the experiment, the bacterial concentration and, thus, the velocity of the colloids are position-dependent as a consequence of the temperature gradient. Then, $v(r)$ is chosen to reproduce the experimental time dynamics of gathering and dispersal shown in Fig. 2.1(f)-(h), (o)-(q): $v(r)$ is constant within the dashed circle in Fig. 2.7(a), $v(r) = 2\ \mu\mathrm{m\,s^{-1}}$, then linearly decays to $v(r) = 1\ \mu\mathrm{m\,s^{-1}}$ at $r = 50\ \mu$m and fades to zero at even longer distances. The optical forces induced by smooth and rough potentials are modeled by imposing an external force field acting on the particles $\mathbf{F} = [F_\mathrm{x}, F_\mathrm{y}]$ [71]: in the case of the smooth optical potential, the forces are calculated as the gradient of a 2D Gaussian potential; while in the case of the random potential, the forces are calculated as the gradient of a 2D speckle intensity pattern with a 2D Gaussian envelope and same average grain size as in the experiments [98, 99, 115]. Inertial effects can be neglected because of the very low Reynolds number regime of our system, while, when a displacement makes two particles overlap, the particles are separated by moving each one half the overlap distance along their centre-to-centre axis. The simulations are robust and the main observable result, that is, the transition from gathering to dispersal of active particles in an attractive potential, depends very little on the particular choice of the parameters (for example, absolute value and functional form of the velocity, and rotational diffusion), although the time dynamics for the two processes can be altered.

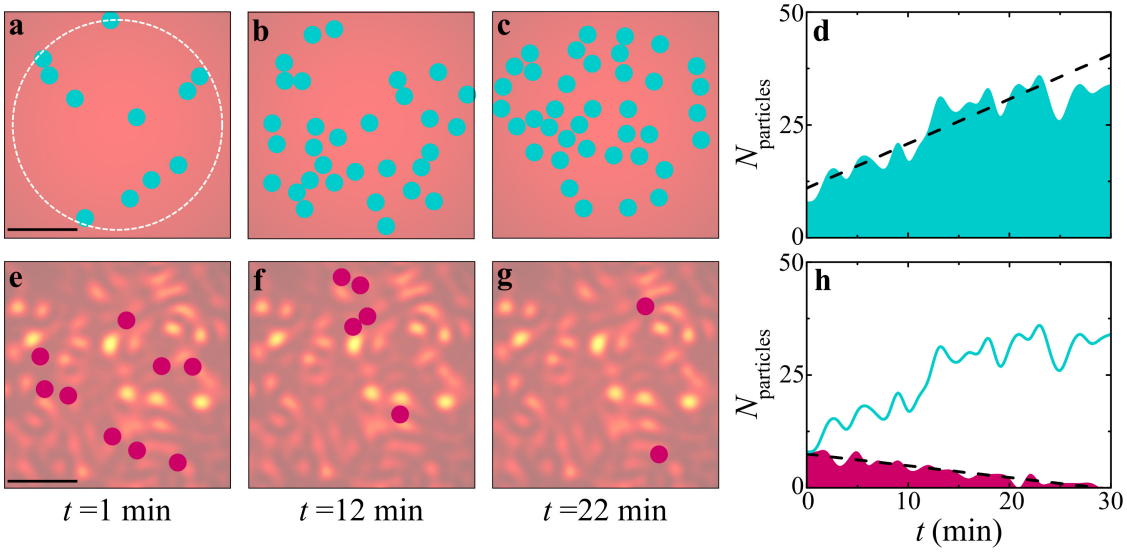

Figure 2.7: Numerical simulations. The (a-c, e-g) time sequences show that active particles gather in a smooth Gaussian potential, while they disperse in a rough spatially disordered potential. The particles move with a position-dependent velocity $v(r)$ that is constant within the dashed circle in a and then fades gradually to zero when radially moving away from it. These simulations are in very good agreement with the experimental time sequences reported in Fig. 2.1 (f)-(h), (o)-(q), respectively. The scale bars correspond to 20 µm. Sample intensity distributions are shown in the background for the two time sequences. The shaded areas in d and h, respectively, show the time evolution of the active particles for the two previous cases. The dashed lines are linear fits whose slopes give the initial rate of particle gathering or dispersal. To directly compare smooth and rough potentials, the time evolution of d is also shown as a solid line in h. The simulation parameters are chosen to closely mimic the corresponding experimental values. Reprint from [104].

2.2.5 Absence of convection and thermophoresis

For our experimental conditions, we can exclude a convection-driven flow for the particles since the Rayleigh number

$$Ra = \frac{g\alpha\Delta T l^3}{\upsilon\kappa} \approx 0.02 \ll 1700, \tag{2.2}$$

where 1700 represents the critical value above which the onset of convection occurs in the Bérnard configuration corresponding to two parallel horizontal boundaries separated by a distance $l = 100$ µm and with a temperature difference $\Delta T = 1.2$ K; $g = 9.8\,\mathrm{m\,s^{-2}}$ is the gravitational acceleration, $\alpha = 2 \cdot 10^{-4}\,\mathrm{K^{-1}}$, is the thermal

expansion coefficient of water, $v = 10^{-6}\,\mathrm{m}^2\ \mathrm{s}^{-1}$ is its thermal diffusivity. Moreover, since silica particles have a positive Soret coefficient, thermophoresis can be excluded because, in absence of bacteria, they would otherwise be pushed away from the warmer central illuminated area towards the colder outside boundaries rather than gathering at its center.

2.2.6 Radial drift calculation

The radial drift $v_r(r)$ quantifies the average velocity at which the colloids move away from the center of the illuminated area along any radial direction, and it is defined as

$$v_{\mathrm{r}}(r) = \frac{1}{\Delta t}\langle r_{\mathrm{n+1}} - r_{\mathrm{n}} \mid r_{\mathrm{n}} \cong r\rangle \tag{2.3}$$

where r_{n} are discrete samples of the radial position of the colloidal particles calculated from the center of the optical beam and Δt is the time step between samples.

Optical Potential	Bath	$r(\mu\mathrm{m})$	$v_{\mathrm{r}}(\mu\mathrm{m\,s}^{-1})$
smooth	thermal	30	-0.37
smooth	active	30	-0.11
rough	thermal	30	-0.26
rough	active	30	$+0.09$

Table 2.1: Radial drift. Radial drift v_{r} at $r = 30$ µm for colloids in thermal and active baths under different potentials. The radial drift is positive only for colloids in an active bath moving on a rough potential.

A negative radial drift means the particles are gathering at the center, while a positive radial drift indicates that the particles are moving away from it. In a thermal bath, the effective radial drift of the colloidal particles is negative both in smooth and rough optical potentials; in an active bath, the radial drift is negative only in a smooth potential, while it is positive in a disordered potential, thus confirming the dispersal of colloids in this case (Table 2.1).

2.2.7 Heating effects

We measured the temperature increase over room temperature (fixed at 23 °C) at the center of the illuminated area (Fig. 2.8) by fluorescence intensity measurements of Rhodamine B (Merck Millipore) using a photodiode [116]. in particular, our sample chamber was filled with a solution of rhodamine B (0.1 mM) prepared in carbonate buffer (0.02 M); all solutions were prepared using deionized water. The calibration curve in Fig. 2.8 is obtained by linearly fitting the data points acquired by measuring the fluorescence intensity of the solution (excitation $\lambda = 532$ nm and $P = 5$ mW to avoid photobleaching) at different temperatures on a microscopy stage with temperature controlled at $\pm$ 0.05 K (using a heat bath). Under laser illumination at $\lambda = 976$ nm ($P = 100$ mW, $w_0 = 47.8 \pm 0.2$ µm brown square), we measured a temperature increase of 1.3 ± 0.3 K. We remark that the absorption coefficient of water at $\lambda = 785$ nm is approximately twenty times smaller than at $\lambda = 976$ nm, thus the temperature variation will also be approximately twenty time smaller for the same power of the illumination, as confirmed from the measurements in Fig. 2.8 where we did not observe any temperature increase at $\lambda = 785$ nm ($P = 100$ mW, $w_0 = 49.9 \pm 0.2$ µm, red circle).

To gain insight on the temperature distribution beyond the spatial resolution of our measurements, for the case of light absorption from the motility buffer in our sample chamber (dimensions $w_{\mathrm{x}} = 1$ mm, $w_{\mathrm{y}} = 1$ mm, $w_{\mathrm{z}} = 1$ mm), we can calculate the temperature variation ΔT above room temperature due to laser illumination by numerically solving the steady-state Fouriers law of heat conduction [117]:

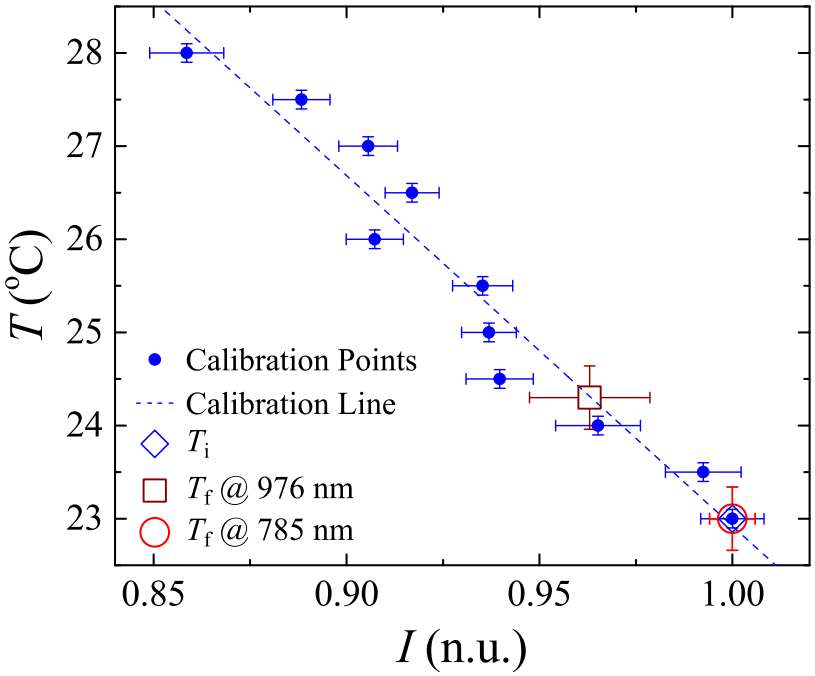

Figure 2.8: Temperature increase measurement. The normalized fluorescence intensity of Rhodamine B solutions in the sample chamber is a sensitive indicator of the sample solution temperature. In absence of laser illumination, the temperature of the sample cell is the room temperature (blue diamond, 23 °C). Under illumination with a laser at $\lambda = 976$ nm ($P = 100$ mW, $w_0 = 47.8$ pm 0.2 µm, brown square) the temperature increases by $\Delta T = 1.3 \pm 0.3$ K. Under illumination with a laser at $\lambda = 785$ nm (P=100 mW, $w_0 = 49.9 \pm 0.2$ µm, red circle) the temperature of the sample does not change appreciably. The dashed line shows the calibration curve that relates fluorescence intensity to temperature used to perform the measurements. This curve is the linear fitting line for the calibration data points (dots). Error bars represent one standard deviation around the mean values averaged over 6 measurements per data point. Reprint from [104].

$$\nabla^2(\Delta T(\mathbf{r})) = -\frac{\mu(\lambda)}{C} I(\mathbf{r}) \tag{2.4}$$

where $I(\mathbf{r})$ is the intensity of the laser beam at point $\mathbf{r}$; $\mu(\lambda)$ is the absorption coefficient of the water in the buffer at a given wavelength; and C is its thermal conductivity. In our case, $I(\mathbf{r})$ is either given by a Gaussian beam or a speckle pattern with a Gaussian envelope, both propagating along z. For water, $\mu(\lambda) = 44.5$ m^{-1} at $\lambda = 976\,$nm , $\mu(\lambda) = 2.22$ m^{-1} at $\lambda = 785\,$nm and $C = 0.60$ W m^{-1} K^{-1}. The intensity $I(\mathbf{r})$ is defined on a discretized lattice (spatial step: 1 µm) so that the total power at any xy-plane is equal to 100 mW (as the effect of absorption is negligible on these length scales). The temperature increases obtained from the numerical simulations shown in Fig. 2.2 are in good agreement with the measured values.

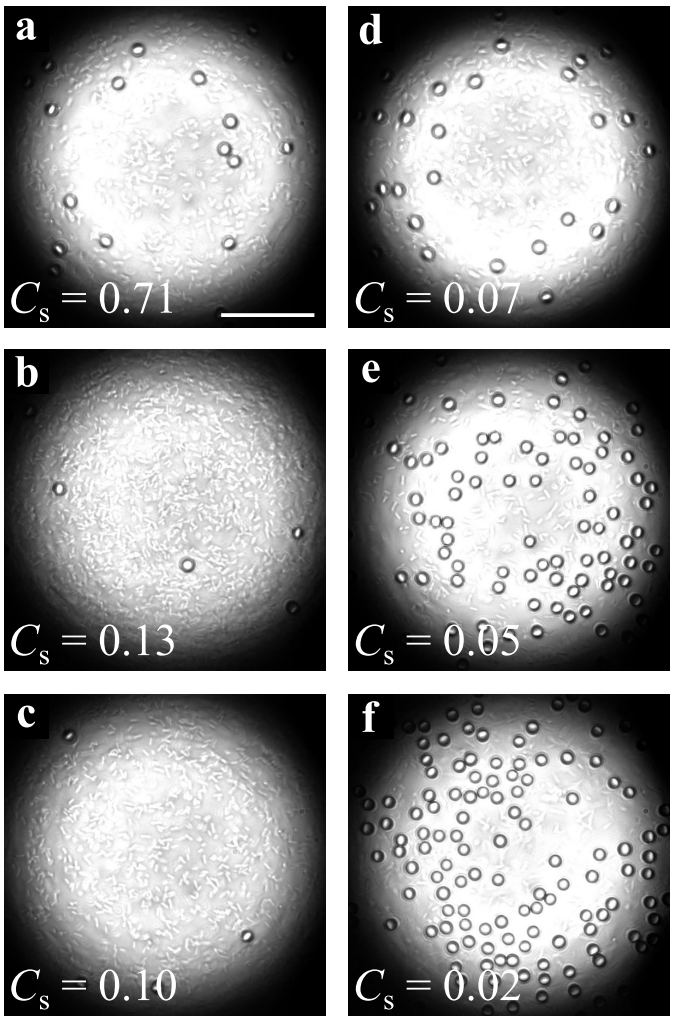

Figure 2.9: Final distribution of colloids for different speckle contrasts. Snapshots at t = 30 minutes of the distribution of colloids in an active bath under different optical potentials where the local roughness is continuously decreased from a high contrast speckle $C_s = 0.71$ (a) to an almost Gaussian distribution with very low speckle contrast $C_s = 0.02$ (f) through four intermediate values (b) $C_s = 0.13$, (c) $C_s = 0.10$, (d) $C_s = 0.07$, (e) $C_s = 0.05$. These snapshots show a non-monotone transition from dispersal (a) to gathering (f) of individuals in the central illuminated area. The scale bar corresponds to 40 µm. The complete time evolutions of the colloidal population are shown in Fig. 2.4(d)-(f) and Fig. 2.4(j)-(l). Reprint from [104].

Chapter 3

Individual and collective motion of bionic microswimmers

As we have seen, self-propelling agents can be defined as controllable microscopic active particles which can harvest energy from the environment and transform it into a self-propulsive motion [4, 43, 118]. Ideally, self-propelling swimmers are expected to autonomously perform a given task inside hardly accessible domains [113, 119]. Various artificial self-propulsion methods have been implemented in order to realize active Brownian motion at the microscale [56]. One of the most common example of such propulsion mechanisms is the chemical activation of a catalytic interaction between microswimmer and the liquid medium; i.e. self-diffusiophoresis through decomposition of H_2O_2 or demixing of a surrounding critical mixture by illumination [42, 43, 81]. The physical mechanism behind this self-propelling action is not fully understood yet and several proposed clarifications include self-electrophoresis [120,121] and oxygen bubble formation [122]. For the study of living active matter systems, using these chemical compounds bring experimental limitations and several drawbacks because catalytic microswimmers can be only activated inside a chemically active region and their byproducts can be physiologically noxious to cells and other organisms. Therefore, environmental factors such as pH, temperature and level of oxygen must be specifically adjusted

for studying living systems *in vivo* and *in vitro*. An alternative approach to create bio-friendly microactuators is using artificial substrates, e.g. colloidal beads anchored by living motile cells [123, 124]. The biohybridization method of swimmers holds a great potential for specific tasks such as targeted delivery performed by bacterial cells where they can be directed and steered through taxis response. *E. coli* [125–127], *Serratia marcescens* [50, 128], phototactic algae [129], magnetotactic bacteria [130] and sperm cells [131] can be tethered to various substrates as small motile organisms in order to control pathways of microactuator transportation and cargo delivery. *S. marcescens* is an opportunistic pathogen and thus not very suitable for such studies and possible biomedical applications. On the other hand, the propulsion mechanism as well as chemotactic response of *E. coli* has been extensively studied and very well-known. Furthermore, the bacterial strains containing non-pathogenic variants of *E. coli* can be safely isolated and replicated in a laboratory environment and they do not possess any harmful effects on human health. Therefore, *E. coli* cells can be readily used in various biophysical studies regarding cell motility [132, 133]. Recently, Sahari *et al.* fabricated a biohybrid microswimmer by attaching *E. coli* bacteria with protein-ligand interaction on the surface of polystyrene(PS) particles [127]. We followed a similar method and protocol to form bionic microswimmers based on motile *E. coli* bacteria. We used streptavidin conjugated spherical melamine resin (MF) particles and biotin conjugated antibodies targeting particular antigenic sites on membrane of the microorganism in order to couple particles with freely swimming *E. coli* cells (section 3.1). We were able to control the average number of bacterial cells attached on a given particle surface by adjusting the dilution rate of the biotin conjugating antibody added into the suspension. As a result, we observed colloidal aggregates in a particle ensemble formed by two or more particles attached to each other. We called these higher colloidal structures as dimers, trimers and so on depending on their colloidal valence number. The attachment method causes bacterial cells to be randomly tethered on a given colloidal surface. Therefore, this creates a unique type of behavior of bionic microswimmers where the motion of the particle is highly dependent on the number of cells attached to it as well as their position on the particle. By using a video microscopy setup and conventional particle tracking methods, we retrieved the trajectory of monomers

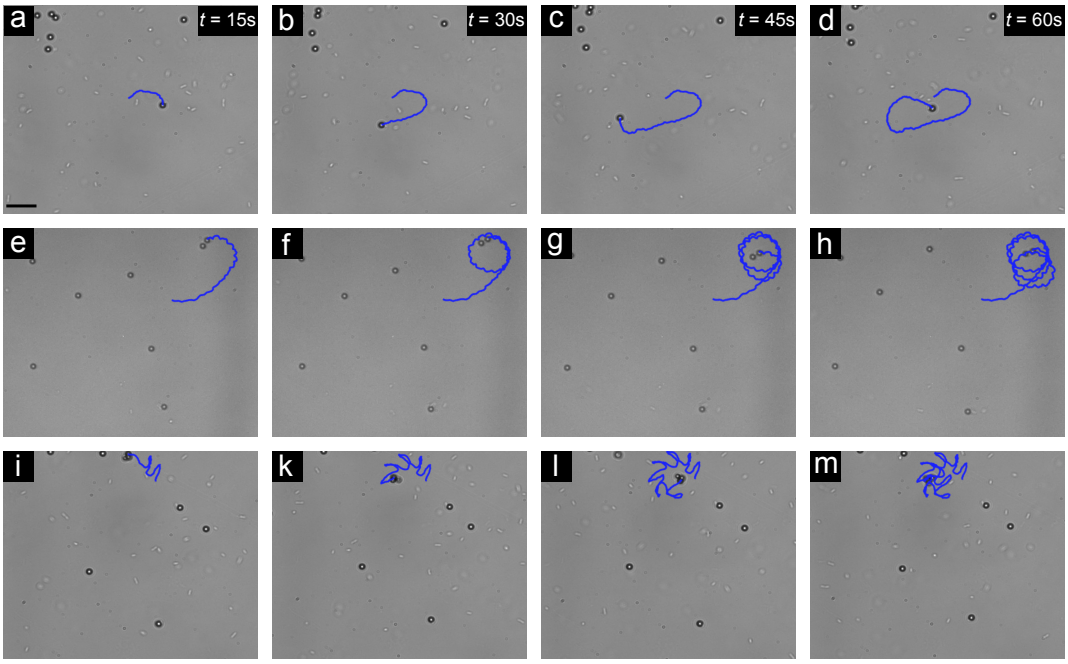

Figure 3.1: Motions of a monomer, dimer and trimer. (a-d) Time sequence of a video shows the trajectory of the active particle (melamine resin(MF) microsphere, $d = 3.27$ µm) attached to a single bacterium (*E. coli*). Trajectories are extracted from a set of video sampled at 10 f.p.s. The scale bar corresponds to 15 µm for each set. The motion of the active monomer clearly shows a chiral (left-handed) character. (e-h) Time sequence of a video showing the trajectory of a dimer. (i-m) Time sequence of a video shows trajectory of a trimer.

attached by a single and double or more *E. coli* cells and calculated their mean square displacement (MSD). Furthermore, we studied the collective dynamics of individual bionic microswimmers. We observed that collection of bionic microswimmers can dynamically form large colloidal aggregates. This phenomenon was previously observed on active Brownian particles [134, 135], light activated artificial microswimmers [45, 81] and motile bacteria [85, 86, 136]. Our model system of active colloids is confined to a quasi-two dimensional sample space due of the hydrodynamic coupling between bacterial flagella and the wall of sample chamber [76].

Monomers, dimers and trimers of active colloids show a characteristic motion depending on the number of colloidal bodies and on the number of bacteria attached to them. Figure 3.1 shows trajectories of each active particle class. The competition between translational and rotational motion on each particle aggregate, from monomer to trimer, shifts the characteristics of the motion from a superdiffusive to a sub-diffusive transport regime. To obtain a better insight into the motion characteristics of each colloidal structure, we calculated the mean-square displacement (MSD) and mean-square angular displacement (MSAD) of each particle type ensemble (Fig. 3.2). Monomer with single and double bacteria shows a superlinear trend for shorter and longer timescales whereas dimer displays oscillatory behavior at longer times. For trimer case, MSD and MSAD data display a sublinear trend which can be estimated as trimer is undergoing sub-diffusional process. The misalignment between rotational and translational of three-body-colloidal aggregates is larger compared to the other particle species, therefore we can claim that the trimer's motion is mostly governed by rotational diffusion. The trajectory data shown in Fig. 3.1(i-m) is supporting this argument: the trimer's trajectory is confined to a smaller area because the average step length is smaller than for the monomer and dimer case within the same time period. This is mainly due to the random bacterial attachment that contributes to the total torque acted on the whole body causing the diversion from a linear trajectory. Ebbens *et al.* previously reported that a dimer of Janus particles display oscillations of MSD and MSAD function similar to the case of our bionic microswimmers [113]. The analytical function for the MSAD of a diffusing particle can be written as

$$< \Delta\theta^2 >= \omega^2 t^2 + 2D_{\mathrm{R}}t \tag{3.1}$$

where ω is the angular velocity of the particle and D_{R} is the rotational diffusion constant. In the bionic microswimmer case, we observed an oscillatory behavior of the MSD and MSAD functions. In contrast to a Janus-particle-based dimer, here, we did not observe any crossover from ballistic to diffusive regime inherently coupled to the oscillatory trend of MSD. However, we proved that the quadratic MSAD expression given in equation (3.1) can be fitted to MSAD data of the dimer for smaller timescales. This shows that a living agent, i.e. motile bacteria, which performs chemotactic motion under the influence of chemical cues,

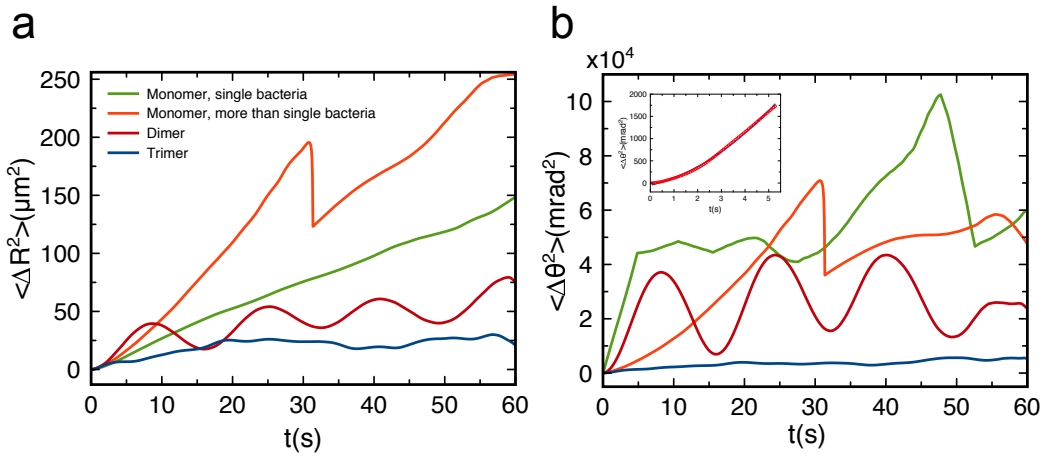

Figure 3.2: Characterization of the motion of bionic microswimmer agglomerate. (a) Mean square displacement of each species of bionic microswimmers shown in Fig 3.1. (b) Mean square angular displacement of bionic microswimmers. The dimer clearly shows an oscillatory behavior. The inset displays MSAD for smaller time-scales(red marker); the fitting function (blue line) follows quadratic increase in time showing a consistent trend with MSAD model for active dimers only for the first five seconds of the experimental time.

follows the same analytical MSAD function as catalytically-activated dimers for a smaller time scale [41]. For the second part of this work, we focused on the collective dynamics of bionic microswimmers. We started by tracking an ensemble of monomers, dimers and trimers of bionic microswimmers and observed that each particle swims and sticks to the neighboring microswimmers, eventually agglomerating into large clusters of swimming particles (Fig. 3.3). This effect is mainly based on the sticky nature of each colloid because of the biomolecules (proteins) present on the colloidal surfaces. The dynamics of cluster formation, however, exhibits similar characteristics to previously reported experiments on artificially activated microswimmers. The main difference between clustering of these bionic microswimmers and chemically activated active particles is the absence of repulsive forces in bionic microswimmer case. Here, the main driving force of the aggregation is the sticky boundary condition imposed upon each colloid by the surrounding active clusters: once a particle reaches a proximity threshold, it is trapped by the agglomerate and it collects other active particles in the surrounding area.

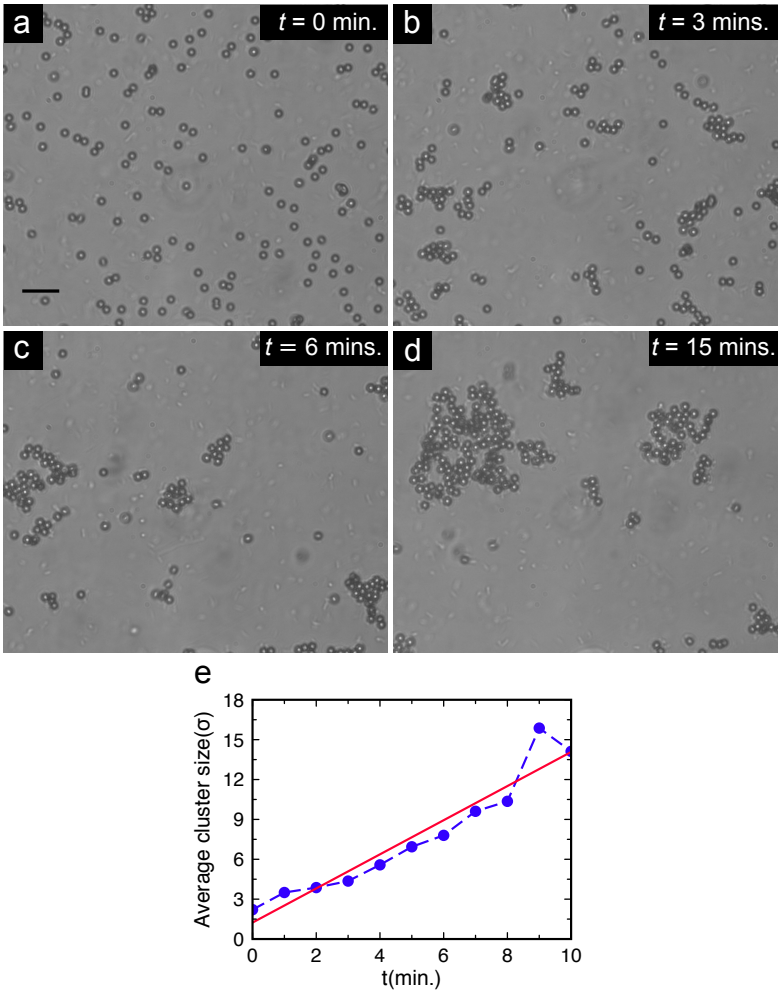

Figure 3.3: Aggregation of bionic microswimmers. (a-d) Time sequence of the video showing the active colloidal clustering. The scale bar corresponds to 15 µm. The trajectory is extracted from a video sampled at 4.55 f.p.s. (e) Average cluster size as a function of experimental time. The linear fit indicates that colloidal clusters grow at a rate of 1.28 particle per minute.

In order to understand and quantify this active sticking effect, we calculated the relative angle distribution $P(\theta, \Delta)$ of the trajectory of a bionic microswimmer stuck by a large colloidal cluster (Fig 3.4). MSD of a particle is not sensitive to the directional features of the particle's motion as an order parameter because it contains only one-dimensional information. Burov *et al.* showed that the relative angle distribution of a given trajectory might probe the complex motion dynamics and provide more information comparing to MSD [137]. This includes the information about how the orientation of a given active particle changes with respect to the caging of the particle by other surrounding particles or geometrical features present in the environment. Here, we calculated the relative angle distribution of the tracer bionic microswimmer to quantify the sticking effect of large colloidal agglomerates. We used the definition of relative angle $\theta(t; \Delta)$

$$\theta(t; \Delta) = \arccos \left[\frac{\mathbf{V}(t; \Delta) \cdot \mathbf{V}(t + \Delta; \Delta)}{|\mathbf{V}(t; \Delta)\|\mathbf{V}(t + \Delta; \Delta)|} \right] \tag{3.2}$$

where $\mathbf{V}(t, \Delta) = \mathbf{X}(t + \Delta) - \mathbf{X}(t)$, the vector between points separated by Δ steps in time domain, $\mathbf{X}(t)$ is the position of the particle at time t and Δ is the lag time between the time steps of a given trajectory. We calculated the probability density function $P(\theta; \Delta)$ by building an histogram of the angle distribution $\theta(t; \Delta)$ for the different values of the lag time Δ.

For the particle shown in Fig. 3.4(a-d), we calculated the relative angle distribution $P(\theta; \Delta)$ (Fig. 3.4(f)). As we increase the value of Δ, the relative angle distribution curve starts to localize around $\theta = \pi$. This effect shows that the set of points in the particle's trajectory marked at smaller time scales becomes anti-correlated with the points marked in the particle's trajectory at longer time scales (Fig 3.4(e)). The particle started its trajectory by freely swimming in the medium (Fig. 3.4(a)) and then it was stuck in the large colloidal agglomerate. The motion of the particle undergoes a transition from superdiffusive to subdiffusive regime. We quantified this effect by calculating the relative angle distribution for two different lag times $\Delta = 2$ and $\Delta = 100$ (Fig 3.4(f)). The peak on the relative angle distribution curve shown in Fig 3.4(f) display a clear shift towards $\theta = \pi$ showing that the motion of the particle is in ballistic regime for smaller

time scales but undergoes a subdiffusive regime for longer time scales.

We demonstrated that *E. coli* based bionic microswimmers show a similar motion characteristics to its artificial counterparts. We calculated the MSD and MSAD functions of each agglomerate up to the trimers and observed that the motion of dimers exhibit a large translational and rotational coupling in their motion as a result of the competition between linear and angular velocity. For the collective dynamics in the bionic microswimmers, we observed the formation of large colloidal aggregates starting from single bionic microswimmer, i.e. monomers. The phenomenon has a striking resemblance to the clustering of light-activated artificial microswimmers.

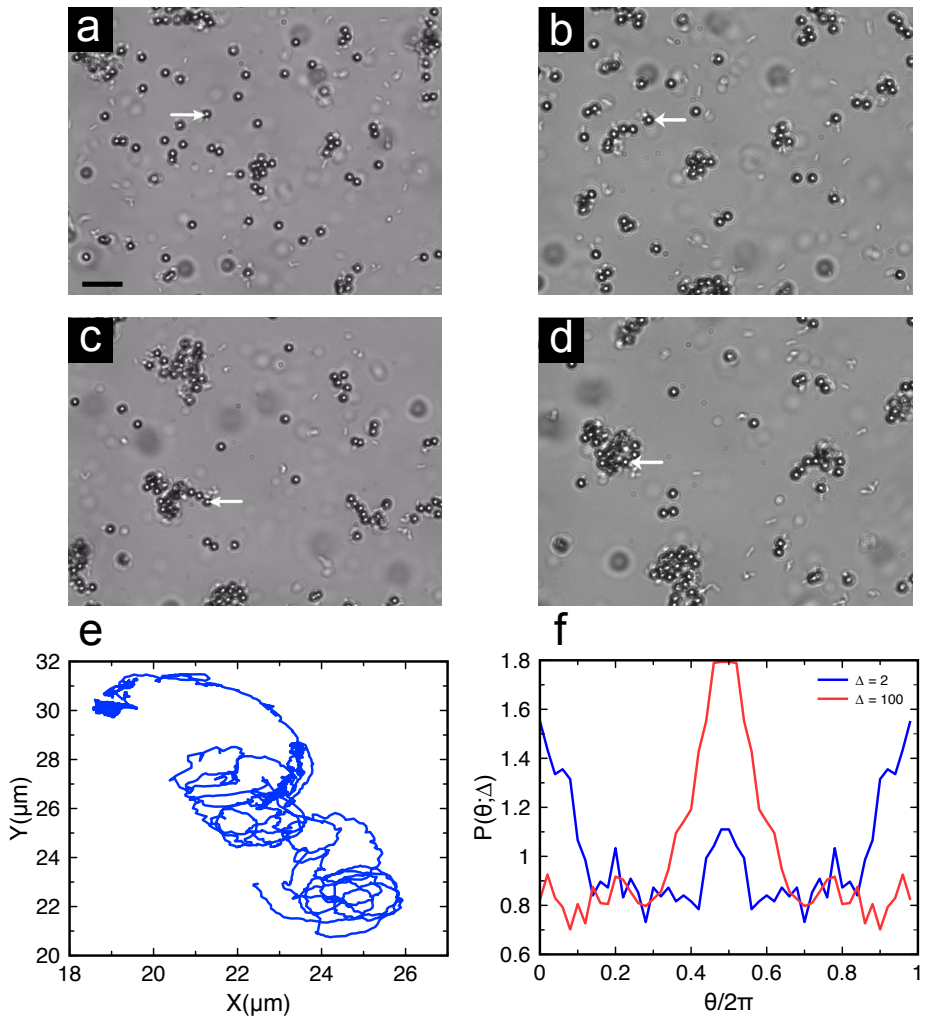

Figure 3.4: Trapping of a single active colloidal particle inside bionic microswimmer cluster. (a-d) Time sequence of a video showing a monomer joining a large cluster of bionic microswimmers. The position of the monomer is shown by the white arrow. The scale bar corresponds to 15 μm. (e) The trajectory of the colloid is extracted from the video sampled at 14.22 f.p.s. The trace of the colloidal particle displays the trapping effect of the cluster as the set of points on monomer's trajectory becomes highly localized inside the agglomerate. (f) Relative angle distribution of points extracted from the monomer. As the lag time Δ is increased, the de-correlation between points at different regions of the trajectory increases and the distribution is shifted towards the center.

3.1 Materials and methods

3.1.1 Experimental setup

For obtaining particle images, we used a home-made inverted microscopy setup with an objective of 20x magnification. We used a white LED as a light source. A CCD camera by Thorlabs captured the pictures showing the sample chamber on 1224 x 1024 pixels at 15 f.p.s.

3.1.2 Culturing bacteria

Bacteria cells (*Escherichia Coli*) were cultured from the wild-type strain-, RP437 provided by *E. coli* Genetic Stock Center at Yale University [138]. The liquid culture of RP437 was taken from -80° C archive stock and streaked onto a fresh sterile hard agar medium. The inoculated Agar plate was incubated and grown overnight at 32.5°C. Single colonies grown upon agar were isolated by sterile toothpicking and inoculated into fresh liquid growth medium containing tryptone broth (1% tryptone). After reaching the saturation phase, the culture was diluted 1:100 into fresh tryptone broth. The final dilution was incubated at 32.5°C and mildly shaken at 180 rpm until the culture reached its middle growth phase (OD600 $\sim$ 0.40). Then, 5 mL volume of the final dilution was transferred into a falcon tube and centrifuged at 2000 rpm at 24°C for 10 min. Precipitated RP437 pellets were then gently collected and immersed in 5 mL of motility buffer containing 10 mM Monobasic Potassium Phosphate (KH_2PO_4), 0.1 mM EDTA, 10 mM Dextrose (Glucose) and 0.002% of Tween 20. The cell-washing procedure was repeated three times in order to undermine the growth medium and terminate further cell duplication inside the motility buffer.

3.1.3 Particle preparation

We used melamine resin (MF) particles produced by "Microparticles GmbH" with a diameter of 3.27 µm, MF particles are diluted from their master stock solution down to a volume fraction of 1%. We added 4 µLs of FITC conjugated streptavidin into the suspension to decorate particles with streptavidin. The suspension mix was incubated on a vortex shaker at 500 rpm, at room temperature for 120 minutes. In order to undermine possible artifacts due to uncoupled streptavidin in the next steps, the particles were centrifuged at $1250g$ for 15 minutes and then resuspended inside 1mL of fresh motility buffer. This washing procedure was repeated five times. For obtaining samples in which we observed single particles, we blocked the particle surface by using bovine serum albumine(BSA) in order to prevent clustering of particles because of non-specific protein-to-protein attachment. Pellets of MF particles are added into 1mL of BSA solution (5%) and incubated at 500 rpm for 30 minutes. BSA-decorated particles were centrifuged at $1250g$ for 15 mins and resuspended inside 1mL of fresh motility buffer. This washing procedure was repeated for three times.

3.1.4 Assembly of bionic microswimmers

We started the assemby of bionic microswimmer by decorating *E. coli* cells. 2mL of cell suspension, which had been washed and resuspended in 5mL of motility buffer, was transferred into an empty 2mL sample tube. This suspension was centrifuged at $750g$ for 10 minutes. Then the resulting pellets were transferred into 1mL of fresh motility buffer. We functionalized *E. coli* cells with primary and biotin-conjugated secondary antibodies in order to anchor them onto MF particle surface. For this purpose, we followed a common antibody blotting protocol: we added 1µL of lipopolysaccharide (LPS) anti-lipid A as primary antibody into 1mL of prepared bacterial suspension and incubated at 500 rpm, room temperature for 10 minutes. Bacterial cells are centrifuged at $750g$ for 10 minutes and resulting pellets were transferred into 1mL of fresh motility buffer. This washing procedure is repeated five times. The dilution rate of biotin conjugated secondary antibody

(Donkey anti-goat IgG) was varied, e.g. from $1:10^3$ to $1:10^4$, in order to control the amount of bacterial cells attached over MF bead surfaces. We incubated the bacterial suspension containing biotin-conjugated secondary antibody at 500 rpm. for 10 minutes. Then, bacterial cells are centrifuged at $750g$ for 10 minutes and resulting pellets were transferred into 1mL of fresh motility buffer. This washing procedure is repeated five times to remove excess amount of uncoupled antibodies inside the suspension. At the final step, MF particle suspension was centrifuged at $1250g$, room temperature for 15 minutes and the resulting pellets were suspended inside 1mL of fresh motility buffer and the pellets of *E. coli* cells that had been centrifuged at $750g$, room temperature for 10 minutes was suspended inside this last MF particle solution. Final particle-bacteria mix was incubated at 500 rpm, room temperature for 10 minutes.

Chapter 4

Summary and Outlook

In this thesis, we studied the motion of active matter in complex and crowded environment. At the first part, we studied living active matter as a far-from-equilibrium system and we showed that the dynamics of self-organization in such a dissipative system can be highly sensitive to the environmental conditions. It has been recently showed that spatial disorder can strongly influence the motility of active particles and therefore the presence of noise may alter the dynamics of the collective behavior [96, 97]. Essentially, we studied long-term spatial organization of a colloidal active matter system under two different environmental conditions: smooth and noisy optical potential landscapes. For the smooth optical potential configuration, we generated Gaussian beam and for the noisy optical potential configuration we generated speckle light field pattern by mode-mixing a coherent laser beam in a multimode optical fibre. Here, the active matter system was formed by motile bacterial cells (*E. coli*) and micron-sized silica beads swimming under one of these optical configurations. We showed that colloids swimming in the same environment along with *E. coli* are dispersed away as the optical potential is switched to speckle light field, i.e. the environment is rendered into a spatially disordered state. Furthermore, we gradually controlled the degree of the disorder in the environment by decreasing the potential depth in the speckle light field and we observed the transition from the dispersal of colloids towards their gathering at the central area. We demonstrated that it is possible

to control and switch the spatial configuration of a colloidal active matter system via introducing disordered optical potentials.

In the second part, we studied the motion of a new class of colloidal active particles, bionic microswimmers. Colloidal particles have been a good model system to study and understand the dynamics of self assembly and how the collective motion leads to complex structures in a coordinated fashion [20]. We fabricated bionic microswimmers by decorating the surface of melamine particles with bacterial cells (*E. coli*) through protein-ligand (streptavidin-biotin) interaction. In order to fully understand and quantify how bionic microswimmers move, we studied the colloidal motion in quasi-two dimensional space and observed particle self-assembly formed by basic building blocks of single or double colloids. We classified and characterized trajectories of each type of bionic microswimmer agglomerate from a single body up to higher order structures. Finally, we demonstrated that bionic microswimmers can agglomerate in large swimming colloidal structures. Our work underscores the self-organization capability of *E. coli* based bionic microswimmers to form active particle aggregates.

Bibliography

[1] R. P. Feynman, R. B. Leighton, and M. Sands, *The Feynman Lectures on Physics, Desktop Edition Volume I*, vol. 1. Basic books, 2013.

[2] M. Marchetti, J. Joanny, S. Ramaswamy, T. Liverpool, J. Prost, M. Rao, and R. A. Simha, "Hydrodynamics of soft active matter," *Reviews of Modern Physics*, vol. 85, no. 3, p. 1143, 2013.

[3] S. Ramaswamy, "The mechanics and statistics of active matter," *arXiv preprint arXiv:1004.1933*, 2010.

[4] C. Bechinger, R. Di Leonardo, H. Löwen, C. Reichhardt, G. Volpe, and G. Volpe, "Active brownian particles in complex and crowded environments," *Reviews of Modern Physics*, 2016.

[5] E. Schrödinger, *What is life?: With mind and matter and autobiographical sketches*. Cambridge University Press, 1992.

[6] L. Boltzmann and S. G. Brush, *Vorlesungen über Gastheorie*, vol. 1. Akademische Druck-u. Verlagsanstalt, 1981.

[7] G. Nicolis, I. Prigogine, *et al.*, *Self-organization in nonequilibrium systems*, vol. 191977. Wiley, New York, 1977.

[8] H. Haken, *Information and self-organization: A macroscopic approach to complex systems*. Springer Science & Business Media, 2006.

[9] S. Academy, *General Chemistry: Principles, Patterns, and Applications General Chemistry: Principles, Patterns, and Applications*. Saylor Academy, 2012.

[10] W. Kauzmann, "The nature of the glassy state and the behavior of liquids at low temperatures.," *Chemical Reviews*, vol. 43, no. 2, pp. 219–256, 1948.

[11] T. A. Witten and L. M. Sander, "Diffusion-limited aggregation," *Physical Review B*, vol. 27, no. 9, p. 5686, 1983.

[12] P. Meakin, "Formation of fractal clusters and networks by irreversible diffusion-limited aggregation," *Physical Review Letters*, vol. 51, no. 13, p. 1119, 1983.

[13] B. P. Belousov, "A periodic reaction and its mechanism," *Compilation of Abstracts on Radiation Medicine*, vol. 147, no. 145, p. 1, 1959.

[14] V. K. Vanag and I. R. Epstein, "Pattern formation in a tunable medium: The belousov-zhabotinsky reaction in an aerosol ot microemulsion," *Physical review letters*, vol. 87, no. 22, p. 228301, 2001.

[15] K. Sneppen, "Self-organized pinning and interface growth in a random medium," *Physical review letters*, vol. 69, no. 24, p. 3539, 1992.

[16] H. E. Stanley, "Introduction to phase transitions and critical phenomena," *Introduction to Phase Transitions and Critical Phenomena, by H Eugene Stanley, pp. 336. Foreword by H Eugene Stanley. Oxford University Press, Jul 1987. ISBN-10: 0195053168. ISBN-13: 9780195053166*, vol. 1, 1987.

[17] G. Ahlers, S. Grossmann, and D. Lohse, "Heat transfer and large scale dynamics in turbulent rayleigh-bénard convection," *Reviews of modern physics*, vol. 81, no. 2, p. 503, 2009.

[18] N. A. Clark, A. J. Hurd, and B. J. Ackerson, "Single colloidal crystals," *Nature*, 1979.

[19] P. Pieranski, "Colloidal crystals," *Contemporary Physics*, vol. 24, no. 1, pp. 25–73, 1983.

[20] V. N. Manoharan, "Colloidal matter: Packing, geometry, and entropy," *Science*, vol. 349, no. 6251, p. 1253751, 2015.

[21] J.-M. Lehn, "Perspectives in supramolecular chemistry—from molecular recognition towards molecular information processing and self-organization," *Angewandte Chemie International Edition in English*, vol. 29, no. 11, pp. 1304–1319, 1990.

[22] J.-M. Lehn, "Toward self-organization and complex matter," *Science*, vol. 295, no. 5564, pp. 2400–2403, 2002.

[23] V. Percec, M. Glodde, T. Bera, Y. Miura, I. Shiyanovskaya, K. Singer, V. Balagurusamy, P. Heiney, I. Schnell, A. Rapp, *et al.*, "Self-organization of supramolecular helical dendrimers into complex electronic materials," *Nature*, vol. 419, no. 6905, pp. 384–387, 2002.

[24] A. M. Turing, "The chemical basis of morphogenesis," *Philosophical Transactions of the Royal Society of London B: Biological Sciences*, vol. 237, no. 641, pp. 37–72, 1952.

[25] E. Ben-Jacob, H. Shmueli, O. Shochet, and A. Tenenbaum, "Adaptive self-organization during growth of bacterial colonies," *Physica A: Statistical Mechanics and its Applications*, vol. 187, no. 3, pp. 378–424, 1992.

[26] A. Czirók, E. Ben-Jacob, I. Cohen, and T. Vicsek, "Formation of complex bacterial colonies via self-generated vortices," *Physical Review E*, vol. 54, no. 2, p. 1791, 1996.

[27] E. Ben-Jacob, I. Cohen, and H. Levine, "Cooperative self-organization of microorganisms," *Advances in Physics*, vol. 49, no. 4, pp. 395–554, 2000.

[28] I. D. Couzin and J. Krause, "Self-organization and collective behavior in vertebrates," *Advances in the Study of Behavior*, vol. 32, pp. 1–75, 2003.

[29] T. Vicsek and A. Zafeiris, "Collective motion," *Physics Reports*, vol. 517, no. 3, pp. 71–140, 2012.

[30] C. W. Reynolds, "Flocks, herds and schools: A distributed behavioral model," *ACM SIGGRAPH computer graphics*, vol. 21, no. 4, pp. 25–34, 1987.

[31] T. Vicsek, A. Czirók, E. Ben-Jacob, I. Cohen, and O. Shochet, "Novel type of phase transition in a system of self-driven particles," *Physical review letters*, vol. 75, no. 6, p. 1226, 1995.

[32] A. Czirók, H. E. Stanley, and T. Vicsek, "Spontaneously ordered motion of self-propelled particles," *Journal of Physics A: Mathematical and General*, vol. 30, no. 5, p. 1375, 1997.

[33] Y. Tu, "Phases and phase transitions in flocking systems," *Physica A: Statistical Mechanics and its Applications*, vol. 281, no. 1, pp. 30–40, 2000.

[34] J. Toner, Y. Tu, and S. Ramaswamy, "Hydrodynamics and phases of flocks," *Annals of Physics*, vol. 318, no. 1, pp. 170–244, 2005.

[35] H. Levine, W.-J. Rappel, and I. Cohen, "Self-organization in systems of self-propelled particles," *Physical Review E*, vol. 63, no. 1, p. 017101, 2000.

[36] A. Czirók and T. Vicsek, "Collective behavior of interacting self-propelled particles," *Physica A: Statistical Mechanics and its Applications*, vol. 281, no. 1, pp. 17–29, 2000.

[37] J. Barré, R. Chétrite, M. Muratori, and F. Peruani, "Motility-induced phase separation of active particles in the presence of velocity alignment," *Journal of Statistical Physics*, vol. 158, no. 3, pp. 589–600, 2015.

[38] A. Morin, N. Desreumaux, J.-B. Caussin, and D. Bartolo, "Distortion and destruction of colloidal flocks in disordered environments," *Nature Physics*, 2016.

[39] W. F. Paxton, K. C. Kistler, C. C. Olmeda, A. Sen, S. K. St. Angelo, Y. Cao, T. E. Mallouk, P. E. Lammert, and V. H. Crespi, "Catalytic nanomotors: autonomous movement of striped nanorods," *Journal of the American Chemical Society*, vol. 126, no. 41, pp. 13424–13431, 2004.

[40] J. R. Howse, R. A. Jones, A. J. Ryan, T. Gough, R. Vafabakhsh, and R. Golestanian, "Self-motile colloidal particles: from directed propulsion to random walk," *Physical review letters*, vol. 99, no. 4, p. 048102, 2007.

[41] S. J. Ebbens and J. R. Howse, "Direct observation of the direction of motion for spherical catalytic swimmers," *Langmuir*, vol. 27, no. 20, pp. 12293–12296, 2011.

[42] G. Volpe, I. Buttinoni, D. Vogt, H.-J. Kümmerer, and C. Bechinger, "Microswimmers in patterned environments," *Soft Matter*, vol. 7, no. 19, pp. 8810–8815, 2011.

[43] I. Buttinoni, G. Volpe, F. Kümmel, G. Volpe, and C. Bechinger, "Active brownian motion tunable by light," *Journal of Physics: Condensed Matter*, vol. 24, no. 28, p. 284129, 2012.

[44] F. Kümmel, B. ten Hagen, R. Wittkowski, I. Buttinoni, R. Eichhorn, G. Volpe, H. Löwen, and C. Bechinger, "Circular motion of asymmetric self-propelling particles," *Physical review letters*, vol. 110, no. 19, p. 198302, 2013.

[45] J. Palacci, S. Sacanna, A. P. Steinberg, D. J. Pine, and P. M. Chaikin, "Living crystals of light-activated colloidal surfers," *Science*, vol. 339, no. 6122, pp. 936–940, 2013.

[46] J. Palacci, S. Sacanna, S.-H. Kim, G.-R. Yi, D. Pine, and P. Chaikin, "Light-activated self-propelled colloids," *Philosophical Transactions of the Royal Society of London A: Mathematical, Physical and Engineering Sciences*, vol. 372, no. 2029, p. 20130372, 2014.

[47] J. Palacci, S. Sacanna, A. Abramian, J. Barral, K. Hanson, A. Y. Grosberg, D. J. Pine, and P. M. Chaikin, "Artificial rheotaxis," *Science advances*, vol. 1, no. 4, p. e1400214, 2015.

[48] S. Palagi, A. G. Mark, S. Y. Reigh, K. Melde, T. Qiu, H. Zeng, C. Parmeggiani, D. Martella, A. Sanchez-Castillo, N. Kapernaum, *et al.*, "Structured light enables biomimetic swimming and versatile locomotion of photoresponsive soft microrobots," *Nature materials*, 2016.

[49] T. Qiu, T.-C. Lee, A. G. Mark, K. I. Morozov, R. Münster, O. Mierka, S. Turek, A. M. Leshansky, and P. Fischer, "Swimming by reciprocal motion at low reynolds number," *Nature communications*, vol. 5, 2014.

[50] B. Behkam and M. Sitti, "Bacterial flagella-based propulsion and on/off motion control of microscale objects," *Applied Physics Letters*, vol. 90, no. 2, p. 023902, 2007.

[51] J. Zhuang, R. W. Carlsen, and M. Sitti, "ph-taxis of biohybrid microsystems," *Scientific reports*, vol. 5, 2015.

[52] R. Dreyfus, J. Baudry, M. L. Roper, M. Fermigier, H. A. Stone, and J. Bibette, "Microscopic artificial swimmers," *Nature*, vol. 437, no. 7060, pp. 862–865, 2005.

[53] R. C. Tolman, *The principles of statistical mechanics*. Courier Corporation, 1938.

[54] R. Kubo, "The fluctuation-dissipation theorem," *Reports on progress in physics*, vol. 29, no. 1, p. 255, 1966.

[55] L. K. Abdelmohsen, F. Peng, Y. Tu, and D. A. Wilson, "Micro-and nanomotors for biomedical applications," *Journal of Materials Chemistry B*, vol. 2, no. 17, pp. 2395–2408, 2014.

[56] S. Ebbens, "Active colloids: Progress and challenges towards realising autonomous applications," *Current Opinion in Colloid & Interface Science*, vol. 21, pp. 14–23, 2016.

[57] D. Patra, S. Sengupta, W. Duan, H. Zhang, R. Pavlick, and A. Sen, "Intelligent, self-powered, drug delivery systems," *Nanoscale*, vol. 5, no. 4, pp. 1273–1283, 2013.

[58] W. Gao and J. Wang, "The environmental impact of micro/nanomachines: a review," *Acs Nano*, vol. 8, no. 4, pp. 3170–3180, 2014.

[59] J. Li, V. V. Singh, S. Sattayasamitsathit, J. Orozco, K. Kaufmann, R. Dong, W. Gao, B. Jurado-Sanchez, Y. Fedorak, and J. Wang, "Water-driven micromotors for rapid photocatalytic degradation of biological and chemical warfare agents," *ACS nano*, vol. 8, no. 11, pp. 11118–11125, 2014.

[60] R. Brown, "Xxvii. a brief account of microscopical observations made in the months of june, july and august 1827, on the particles contained in the pollen of plants; and on the general existence of active molecules in organic and inorganic bodies," *Philosophical Magazine Series 2*, vol. 4, no. 21, pp. 161–173, 1828.

[61] A. Fick, "Ueber diffusion," *Annalen der Physik*, vol. 170, no. 1, pp. 59–86, 1855.

[62] A. Einstein, "Über die von der molekularkinetischen theorie der wärme geforderte bewegung von in ruhenden flüssigkeiten suspendierten teilchen," *Annalen der physik*, vol. 322, no. 8, pp. 549–560, 1905.

[63] M. Von Smoluchowski, "Zur kinetischen theorie der brownschen molekularbewegung und der suspensionen," *Annalen der physik*, vol. 326, no. 14, pp. 756–780, 1906.

[64] W. Sutherland, "Lxxv. a dynamical theory of diffusion for non-electrolytes and the molecular mass of albumin," *The London, Edinburgh, and Dublin Philosophical Magazine and Journal of Science*, vol. 9, no. 54, pp. 781–785, 1905.

[65] A. Einstein, *Investigations on the Theory of the Brownian Movement*. Courier Corporation, 1956.

[66] P. N. Pusey, "Brownian motion goes ballistic," *Science*, vol. 332, no. 6031, pp. 802–803, 2011.

[67] T. Li, S. Kheifets, D. Medellin, and M. G. Raizen, "Measurement of the instantaneous velocity of a brownian particle," *Science*, vol. 328, no. 5986, pp. 1673–1675, 2010.

[68] R. Huang, I. Chavez, K. M. Taute, B. Lukić, S. Jeney, M. G. Raizen, and E.-L. Florin, "Direct observation of the full transition from ballistic to diffusive brownian motion in a liquid," *Nature Physics*, vol. 7, no. 7, pp. 576–580, 2011.

[69] M. G. Raizen and T. Li, "The measurement einstein deemed impossible," *Physics Today*, vol. 68, no. 1, p. 56, 2015.

[70] G. Volpe and G. Volpe, "Simulation of a brownian particle in an optical trap," *American Journal of Physics*, vol. 81, no. 3, pp. 224–230, 2013.

[71] G. Volpe, S. Gigan, and G. Volpe, "Simulation of the active brownian motion of a microswimmer," *American Journal of Physics*, vol. 82, no. 7, pp. 659–664, 2014.

[72] H. S. Jennings, "On the significance of the spiral swimming of organisms," *The American Naturalist*, vol. 35, no. 413, pp. 369–378, 1901.

[73] E. Lauga and T. R. Powers, "The hydrodynamics of swimming microorganisms," *Reports on Progress in Physics*, vol. 72, no. 9, p. 096601, 2009.

[74] J. Elgeti, R. G. Winkler, and G. Gompper, "Physics of microswimmers—single particle motion and collective behavior: a review," *Reports on progress in physics*, vol. 78, no. 5, p. 056601, 2015.

[75] S. Mathur, M. Carlton, J. Ziegler, P. F. Rust, and H. O. Williamson, "A computerized sperm motion analysis," *Fertility and sterility*, vol. 46, no. 3, pp. 484–488, 1986.

[76] E. Lauga, W. R. DiLuzio, G. M. Whitesides, and H. A. Stone, "Swimming in circles: motion of bacteria near solid boundaries," *Biophysical journal*, vol. 90, no. 2, pp. 400–412, 2006.

[77] R. Di Leonardo, D. Dell'Arciprete, L. Angelani, and V. Iebba, "Swimming with an image," *Physical Review Letters*, vol. 106, no. 3, p. 038101, 2011.

[78] O. Sipos, K. Nagy, R. Di Leonardo, and P. Galajda, "Hydrodynamic trapping of swimming bacteria by convex walls," *Physical review letters*, vol. 114, no. 25, p. 258104, 2015.

[79] W. R. DiLuzio, L. Turner, M. Mayer, P. Garstecki, D. B. Weibel, H. C. Berg, and G. M. Whitesides, "Escherichia coli swim on the right-hand side," *Nature*, vol. 435, no. 7046, pp. 1271–1274, 2005.

[80] M. Mijalkov and G. Volpe, "Sorting of chiral microswimmers," *Soft Matter*, vol. 9, no. 28, pp. 6376–6381, 2013.

[81] I. Buttinoni, J. Bialké, F. Kümmel, H. Löwen, C. Bechinger, and T. Speck, "Dynamical clustering and phase separation in suspensions of self-propelled colloidal particles," *Physical review letters*, vol. 110, no. 23, p. 238301, 2013.

[82] Y. Fily and M. C. Marchetti, "Athermal phase separation of self-propelled particles with no alignment," *Physical review letters*, vol. 108, no. 23, p. 235702, 2012.

[83] J. Tailleur and M. Cates, "Statistical mechanics of interacting run-and-tumble bacteria," *Physical review letters*, vol. 100, no. 21, p. 218103, 2008.

[84] M. E. Cates and J. Tailleur, "Motility-induced phase separation," *Annu. Rev. Condens. Matter Phys.*, vol. 6, no. 1, pp. 219–244, 2015.

[85] A. P. Petroff, X.-L. Wu, and A. Libchaber, "Fast-moving bacteria self-organize into active two-dimensional crystals of rotating cells," *Physical review letters*, vol. 114, no. 15, p. 158102, 2015.

[86] X. Chen, X. Yang, M. Yang, and H. Zhang, "Dynamic clustering in suspension of motile bacteria," *EPL (Europhysics Letters)*, vol. 111, no. 5, p. 54002, 2015.

[87] A. Mastrobuono-Battisti, H. B. Perets, and S. N. Raymond, "A primordial origin for the compositional similarity between the earth and the moon," *Nature*, vol. 520, no. 7546, pp. 212–215, 2015.

[88] M. Begon, C. R. H. Townsend, L. John, R. T. Colin, and L. H. John, *Ecology: from individuals to ecosystems*. Wiley-Blackwell, 2006.

[89] S. Park, P. M. Wolanin, E. A. Yuzbashyan, P. Silberzan, J. B. Stock, and R. H. Austin, "Motion to form a quorum," *Science*, vol. 301, no. 5630, pp. 188–188, 2003.

[90] F. Farrell, O. Hallatschek, D. Marenduzzo, and B. Waclaw, "Mechanically driven growth of quasi-two-dimensional microbial colonies," *Physical review letters*, vol. 111, no. 16, p. 168101, 2013.

[91] L. Hall-Stoodley, J. W. Costerton, and P. Stoodley, "Bacterial biofilms: from the natural environment to infectious diseases," *Nature reviews microbiology*, vol. 2, no. 2, pp. 95–108, 2004.

[92] H. Salman and A. Libchaber, "A concentration-dependent switch in the bacterial response to temperature," *Nature cell biology*, vol. 9, no. 9, pp. 1098–1100, 2007.

[93] J.-M. Lehn, "Toward complex matter: Supramolecular chemistry and self-organization," *Proceedings of the National Academy of Sciences*, vol. 99, no. 8, pp. 4763–4768, 2002.

[94] T. Sanchez, D. T. Chen, S. J. DeCamp, M. Heymann, and Z. Dogic, "Spontaneous motion in hierarchically assembled active matter," *Nature*, vol. 491, no. 7424, pp. 431–434, 2012.

[95] U. Gasser, "Crystallization in three-and two-dimensional colloidal suspensions," *Journal of Physics: Condensed Matter*, vol. 21, no. 20, p. 203101, 2009.

[96] O. Chepizhko and F. Peruani, "Diffusion, subdiffusion, and trapping of active particles in heterogeneous media," *Physical review letters*, vol. 111, no. 16, p. 160604, 2013.

[97] C. Reichhardt and C. O. Reichhardt, "Active matter transport and jamming on disordered landscapes," *Physical Review E*, vol. 90, no. 1, p. 012701, 2014.

[98] G. Volpe, G. Volpe, and S. Gigan, "Brownian motion in a speckle light field: tunable anomalous diffusion and selective optical manipulation," *Scientific reports*, vol. 4, 2014.

[99] G. Volpe, L. Kurz, A. Callegari, G. Volpe, and S. Gigan, "Speckle optical tweezers: micromanipulation with random light fields," *Optics express*, vol. 22, no. 15, pp. 18159–18167, 2014.

[100] X.-L. Wu and A. Libchaber, "Particle diffusion in a quasi-two-dimensional bacterial bath," *Physical Review Letters*, vol. 84, no. 13, p. 3017, 2000.

[101] H. C. Berg, *E. coli in Motion*. Springer Science & Business Media, 2008.

[102] G. Grégoire, H. Chaté, and Y. Tu, "Active and passive particles: Modeling beads in a bacterial bath," *Physical Review E*, vol. 64, no. 1, p. 011902, 2001.

[103] J. C. Crocker and D. G. Grier, "Methods of digital video microscopy for colloidal studies," *Journal of colloid and interface science*, vol. 179, no. 1, pp. 298–310, 1996.

[104] E. Pinçe, S. K. Velu, A. Callegari, P. Elahi, S. Gigan, G. Volpe, and G. Volpe, "Disorder-mediated crowd control in an active matter system," *Nature communications*, vol. 7, 2016.

[105] J. W. Goodman, "Some fundamental properties of speckle," *JOSA*, vol. 66, no. 11, pp. 1145–1150, 1976.

[106] E. Barkai, Y. Garini, and R. Metzler, "of single molecules in living cells," *Phys. Today*, vol. 65, no. 8, p. 29, 2012.

[107] M. Demir, C. Douarche, A. Yoney, A. Libchaber, and H. Salman, "Effects of population density and chemical environment on the behavior of escherichia coli in shallow temperature gradients," *Physical biology*, vol. 8, no. 6, p. 063001, 2011.

[108] K. Maeda, Y. Imae, J.-I. Shioi, and F. Oosawa, "Effect of temperature on motility and chemotaxis of escherichia coli.," *Journal of bacteriology*, vol. 127, no. 3, pp. 1039–1046, 1976.

[109] H. Salman, A. Zilman, C. Loverdo, M. Jeffroy, and A. Libchaber, "Solitary modes of bacterial culture in a temperature gradient," *Physical review letters*, vol. 97, no. 11, p. 118101, 2006.

[110] M. Schnitzer, S. Block, and H. Berg, "Strategies for chemotaxis mj schnitzer*, sm blockt, hc bergt, em purcell," *Biology of the chemotactic response*, vol. 46, p. 15, 1990.

[111] M. J. Schnitzer, "Theory of continuum random walks and application to chemotaxis," *Physical Review E*, vol. 48, no. 4, p. 2553, 1993.

[112] O. Chepizhko, E. G. Altmann, and F. Peruani, "Optimal noise maximizes collective motion in heterogeneous media," *Physical review letters*, vol. 110, no. 23, p. 238101, 2013.

[113] S. J. Ebbens and J. R. Howse, "In pursuit of propulsion at the nanoscale," *Soft Matter*, vol. 6, no. 4, pp. 726–738, 2010.

[114] G. Pesce, G. Volpe, O. M. Maragó, P. H. Jones, S. Gigan, A. Sasso, and G. Volpe, "Step-by-step guide to the realization of advanced optical tweezers," *JOSA B*, vol. 32, no. 5, pp. B84–B98, 2015.

[115] A. Callegari, M. Mijalkov, A. B. Gököz, and G. Volpe, "Computational toolbox for optical tweezers in geometrical optics," *JOSA B*, vol. 32, no. 5, pp. B11–B19, 2015.

[116] D. Ross, M. Gaitan, and L. E. Locascio, "Temperature measurement in microfluidic systems using a temperature-dependent fluorescent dye," *Analytical chemistry*, vol. 73, no. 17, pp. 4117–4123, 2001.

[117] E. J. Peterman, F. Gittes, and C. F. Schmidt, "Laser-induced heating in optical traps," *Biophysical journal*, vol. 84, no. 2, pp. 1308–1316, 2003.

[118] P. Romanczuk, M. Bär, W. Ebeling, B. Lindner, and L. Schimansky-Geier, "Active brownian particles," *The European Physical Journal Special Topics*, vol. 202, no. 1, pp. 1–162, 2012.

[119] S. Sanchez, L. Soler, and J. Katuri, "Chemically powered micro-and nanomotors," *Angewandte Chemie International Edition*, vol. 54, no. 5, pp. 1414–1444, 2015.

[120] W. Wang, W. Duan, S. Ahmed, T. E. Mallouk, and A. Sen, "Small power: Autonomous nano-and micromotors propelled by self-generated gradients," *Nano Today*, vol. 8, no. 5, pp. 531–554, 2013.

[121] S. Sanchez and M. Pumera, "Nanorobots: The ultimate wireless self-propelled sensing and actuating devices," *Chemistry–An Asian Journal*, vol. 4, no. 9, pp. 1402–1410, 2009.

[122] R. F. Ismagilov, A. Schwartz, N. Bowden, and G. M. Whitesides, "Autonomous movement and self-assembly," *Angewandte Chemie International Edition*, vol. 41, no. 4, pp. 652–654, 2002.

[123] R. W. Carlsen and M. Sitti, "Bio-hybrid cell-based actuators for microsystems," *Small*, vol. 10, no. 19, pp. 3831–3851, 2014.

[124] A. W. Feinberg, "Biological soft robotics," *Annual review of biomedical engineering*, vol. 17, pp. 243–265, 2015.

[125] R. Fernandes, M. Zuniga, F. R. Sassine, M. Karakoy, and D. H. Gracias, "Enabling cargo-carrying bacteria via surface attachment and triggered release," *Small*, vol. 7, no. 5, pp. 588–592, 2011.

[126] A. Sahari, D. Headen, and B. Behkam, "Effect of body shape on the motile behavior of bacteria-powered swimming microrobots (bacteriabots)," *Biomedical microdevices*, vol. 14, no. 6, pp. 999–1007, 2012.

[127] A. Sahari, M. A. Traore, B. E. Scharf, and B. Behkam, "Directed transport of bacteria-based drug delivery vehicles: bacterial chemotaxis dominates particle shape," *Biomedical microdevices*, vol. 16, no. 5, pp. 717–725, 2014.

[128] N. Darnton, L. Turner, K. Breuer, and H. C. Berg, "Moving fluid with bacterial carpets," *Biophysical journal*, vol. 86, no. 3, pp. 1863–1870, 2004.

[129] D. B. Weibel, P. Garstecki, D. Ryan, W. R. DiLuzio, M. Mayer, J. E. Seto, and G. M. Whitesides, "Microoxen: Microorganisms to move microscale loads," *Proceedings of the National Academy of Sciences of the United States of America*, vol. 102, no. 34, pp. 11963–11967, 2005.

[130] S. Martel, C. C. Tremblay, S. Ngakeng, and G. Langlois, "Controlled manipulation and actuation of micro-objects with magnetotactic bacteria," *Applied Physics Letters*, vol. 89, no. 23, p. 233904, 2006.

[131] V. Magdanz, S. Sanchez, and O. G. Schmidt, "Development of a sperm-flagella driven micro-bio-robot," *Advanced Materials*, vol. 25, no. 45, pp. 6581–6588, 2013.

[132] E. Steager, C.-B. Kim, J. Patel, S. Bith, C. Naik, L. Reber, and M. J. Kim, "Control of microfabricated structures powered by flagellated bacteria using phototaxis," *Applied Physics Letters*, vol. 90, no. 26, p. 263901, 2007.

[133] K. E. Peyer, L. Zhang, and B. J. Nelson, "Bio-inspired magnetic swimming microrobots for biomedical applications," *Nanoscale*, vol. 5, no. 4, pp. 1259–1272, 2013.

[134] A. Bricard, J.-B. Caussin, N. Desreumaux, O. Dauchot, and D. Bartolo, "Emergence of macroscopic directed motion in populations of motile colloids," *Nature*, vol. 503, no. 7474, pp. 95–98, 2013.

[135] M. S. D. Wykes, J. Palacci, T. Adachi, L. Ristroph, X. Zhong, M. D. Ward, J. Zhang, and M. J. Shelley, "Dynamic self-assembly of microscale rotors and swimmers," *Soft Matter*, vol. 12, no. 20, pp. 4584–4589, 2016.

[136] J. Schwarz-Linek, C. Valeriani, A. Cacciuto, M. Cates, D. Marenduzzo, A. Morozov, and W. Poon, "Phase separation and rotor self-assembly in active particle suspensions," *Proceedings of the National Academy of Sciences*, vol. 109, no. 11, pp. 4052–4057, 2012.

[137] S. Burov, S. A. Tabei, T. Huynh, M. P. Murrell, L. H. Philipson, S. A. Rice, M. L. Gardel, N. F. Scherer, and A. R. Dinner, "Distribution of directional change as a signature of complex dynamics," *Proceedings of the National Academy of Sciences*, vol. 110, no. 49, pp. 19689–19694, 2013.

[138] J. S. Parkinson, "Complementation analysis and deletion mapping of escherichia coli mutants defective in chemotaxis.," *Journal of Bacteriology*, vol. 135, no. 1, pp. 45–53, 1978.